UNIVERSITY OF NEW MEXICO
ALBUQUERQUE

ENGINEERING EXPERIMENT STATION

Technical Report EE-89

AN APPROACH TO CORRELATE PULSED RADAR AND PHOTOGRAPHIC DATA

By
Nasir Ahmed*
W. W. Koepsel*

* E.E. Dept., Univ. of N.Mex.
Albuquerque, New Mexico

This work performed for
National Aeronautics and Space
Administration Grant NsG 129-61

UNIVERSITY OF NEW MEXICO

Albuquerque

ENGINEERING EXPERIMENT STATION

Technical Report EE-89

AN APPROACH TO CORRELATE PULSED RADAR AND PHOTOGRAPHIC DATA

By

Nasir Ahmed*

W. W. Koepsel*

* E.E. Dept., Univ. of N.Mex.
Albuquerque, New Mexico

This work performed for
National Aeronautics and Space
Administration Grant NsG 129-61

ABSTRACT

18322

This work describes an approach to the study of correlation between pulsed radar and photographic data as a method of supplementing the available statistical information on area-extensive radar scattering surfaces. A measure of the scattered energy is obtained by studying the variance and power spectra of the radar and photographic data. These spectra are obtained by taking the Fourier Transform of the respective autocorrelation functions obtained from the radar and photographic data. Therefore the variance and power spectra are considered for correlation studies.

The results seem to indicate that a correlation between the radar and photographic data depends on the nature of the terrain. This is because there is a strong correlation between the variance and power spectra for a farmland and the correlation for the spectra obtained from residential and industrial areas which are relatively weak. However, it is felt that in order to make any definite statement regarding the extent to which the correlation of these spectra depends on the type of terrain, further investigations of this nature are necessary.

TABLE OF CONTENTS

3

CHAPTER I

INTRODUCTION

A large number of pictures of the moon have been obtained in recent years. These pictures have been used to study several phenomena. To mention a few, one might refer to their use in providing geological information relative to coarse surface small-scale land forms and features, altitudes and slopes of surface features, and in providing information which will help in the selection of landing sites for the future instrumented and manned lunar probes. However, it is felt that such photographic data could be used more effectively in selecting future landing sites as well as in getting better information regarding the surface structure of the moon. A suggested method of accomplishing this is to compare such photographic data with simultaneously obtained radar data.

The Jet Propulsion Laboratory Lunar Program[1], which is supported by the National Aeronautics and Space Administration has two major projects underway. These are Ranger and Surveyor. The Ranger Project is in the flight stage whereas Surveyor is still in hardware development. The equipment of Ranger 3, 4, and 5 spacecrafts includes a radar altimeter to obtain radar reflection data, and a vidicon camera to obtain close-up pictures of the moon's surface. The data obtained in these flights will thus be available for analysis and comparison using the techniques outlined in this thesis.

---

[1]Scientific Experiments for Ranger 3, 4, and 5: Jet Propulsion Laboratory, California Institute of Technology, Pasadena, California; Technical Report No. 32-199.

The basic problem of comparing radar and photographic data is to determine whether a correlation between the two systems exists. Actually, since two different systems (optical and radar) are involved, one speaks of a correlation between certain characteristics of these systems. Although extensive studies have been done individually in these systems, very little information pertaining to procedures linking the two systems is available in the related unclassified literature. It was therefore proposed that some fundamental investigations be conducted in order to determine whether a correlation between the two systems exists with respect to some basis, such as energy, resolution, pulse shape, etc. This thesis is concerned with such correlation studies.

In the radar experiment, a known amount of energy is incident on a part of a terrain and the energy returned from the terrain is stored in some memory device, which may be a strip of film. This memory device is then analyzed statistically in order to determine certain properties of the terrain. On the other hand, in the photographic experiment, a similar situation exists, except that light energy is incident on the terrain and the amount of light energy reflected is stored by a photograph which serves as the memory device in this system. This manner of viewing the two systems does, in some sense of the word, point out the similarity that exists in their operation.

An approach based on the concept of scattered energy is investigated. A measure of the scattered energy is obtained

by studying the variance and the power spectra of the radar and photographic data respectively. These spectra are obtained by taking the Fourier Cosine Transform of the respective auto-correlation functions obtained from the radar and photographic data. Therefore, the variance and power spectra are considered for correlation studies. It is hoped that the results of this investigation will prove useful to correlate radar and photographic data pertaining to the moon, when available from Ranger 3, 4, and 5.

CHAPTER II

THEORETICAL BACKGROUND

A survey of the literature pertaining to the pulsed radar and photographic systems indicates that the concepts of communication theory have been effectively used to explain their behavior. These systems have been studied with respect to ideal communication systems in the respective domains. In what follows, the behavior of these systems will be discussed with respect to a theory developed by Woodward and Davies[2].

In the radar experiment, communication theory is used to determine whether relatively small received signals contain as much information as those of an ideal communication system working with the same signal to noise ratio. If a single target is considered for the sake of simplicity, then the distance to the target is computed to be equal to $\frac{c\tau}{2}$, where, c is the velocity of light and, τ, is the observed time delay. However, this experiment reduces to the problem of locating a single pulse of known shape in a noisy wave-form as far as its associated mathematics is concerned.

Now, if it is desired to locate a pulse of interest exactly in a noisy wave form, then, theoretically an infinite amount of information is required. However, since this is not the situation met with in practice, this leads one to speak of the

---

[2]Woodward, P.M. and Davies, I.L. "Information Theory and Inverse Probability in Telecommunication" Proc. IEE, Vol. 99, Part III, 3, No. 58, March 1952.

process in probabilistic terms. Thus, the most probable time delay is considered and the corresponding probability distribution will be a representation of the information. Woodward and Davies have employed such an approach to study and explain the radar experiment and have suggested the following probability distribution:

$$P(\tau) = k p(\tau)\, e^{\frac{2}{N}\int_{-\infty}^{\infty} W(t)\cdot S(t-\tau)\,dt} \quad ; \qquad (2.1)$$

where

$P(\tau)$ = probability that the time delay is τ,
k = normalizing constant,
N = mean square noise fluctuation per unit bandwidth,
$p(\tau)$ = a priori probability of before making an observation,
$W(t)$ = is the wave form to be analyzed, and
$S(t)$ = is the amplitude of the pulse at zero delay.

From equation 2.1 it follows that

$$\log_e P(\tau) = \log_e [k p(\tau)] + \frac{2}{N}\int_{-\infty}^{\infty} W(t)\cdot S(t-\tau)\,dt \,. \qquad (2.2)$$

Thus Eq. 2.2 may be computed by merely convolving the observed wave form $W(t)$ whose wave shape is known and the transmitted pulse $S(t)$. Experimentally all this implies is that the signal $W(t)$ may be passed through a filter whose kernal or Green's function is $S(-t)$. The kernal or Green's function is merely the impulse response of the filter. Davies has shown[3] that this is an appropriate filter for determining the probability that a signal of known shape exists in a noisy wave-form.

---

[3] Davies, I.L. "On Determining the Presence of Signals in Noise" Proc. Inst. Elec. Engrs., Vol. 99, Part III, 45(1952).

Further implications of the Woodward-Davies theory have been explained by Felgett[4]. In his paper, Felgett shows that the Woodward-Davies theory could be applied without essential change to study the properties of the photographic grain. This has been done on the basis that the process can be described with the help of the convolution integral given by Eq. 2.2. The approach of explaining the properties of the grain will be considered at a later stage as a part of the description of the process of aerial photography.

Aerial photography will be discussed in two stages, namely optics and the photographic process. Concepts of optics are considered to explain the action of the focusing lens of the camera, while the photographic process is included to explain the behavior of the emulsion of the photographic film. An approach involving communication theory will be entertained and it will be shown that the behavior of the lens is analogous to that of a low-pass linear network filter[5]. The behavior of the emulsion will be discussed with respect to its signal-to-noise ratio.

The optical system, which will now be discussed, is valid for the following assuptions:

1. Linearity
2. Invariance

---

[4]Felgett, P. "Concerning Photographic Grain, Signal-to-Noise Ratio and Information" Jour. of the Optical Society of America, Vol. 43, No. 4, April 1953.

[5]O'Neil, E.L. "Selected Topics in Optics and Communication Theory" Physical Res. Lab., Boston Univ., Tech. Note No. 133, pp 25-28.

The first assumption is found to be valid for most lenses but the second may be debated since the point image distribution is not constant over a given image plane. However, Linfoot and Felgett[6] have shown that this change is so slow over the working field that it is a valid approximation to consider it to be broken up into several zones or "isoplanatic patches" over which invariance is preserved. With these assumptions the optical system will be explained with the help of Fig. 2.1.

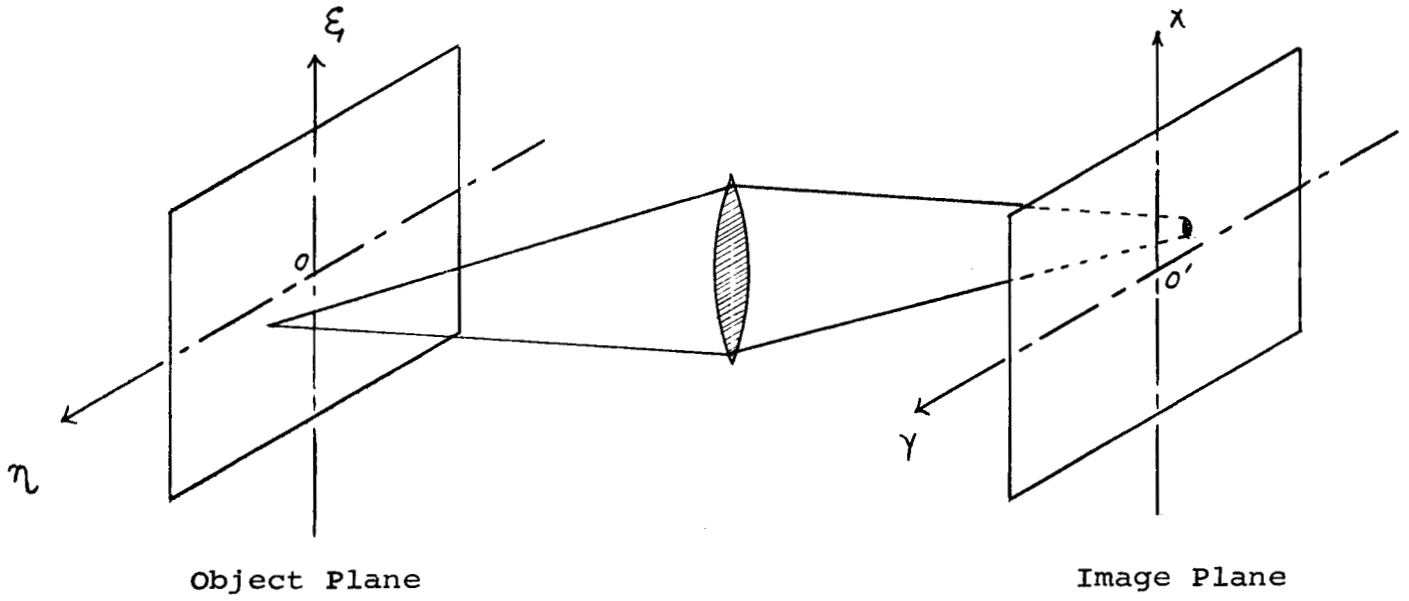

Fig. 2.1. A Representation of the Image and Object Planes.

If $O(\xi,\eta)$ is the object intensity, then, the corresponding image intensity $i(x,y)$ may be expressed as:

$$i(x,y) = A\iint_{-\infty}^{\infty} S(x-\xi, y-\eta)\, O(\xi,\eta)\, d\xi\, d\eta \qquad (2.4)$$

[6]Linfoot, E.H. and Felgett, P.B. "On Assessment of Optical Images" Trans. Roy. Soc. (London), 247, Feb 1955.

A is the magnification (or gain) of the lens.

By the use of two-dimensional Fourier Transforms one may define the following:

$$I(\omega_x,\omega_y) = \frac{A}{2\pi}\iint_{-\infty}^{\infty} i(x,y)\, e^{-i(\omega_x x+\omega_y y)}dxdy, \tag{2.5}$$

$$O(\omega_x,\omega_y) = \frac{A}{2\pi}\iint_{-\infty}^{\infty} o(x,y)\, e^{-i(\omega_x x+\omega_y y)}dxdy, \tag{2.6}$$

$$S(\omega_x,\omega_y) = \frac{A}{2\pi}\iint_{-\infty}^{\infty} s(x,y)\, e^{-i(\omega_x x+\omega_y y)}dxdy. \tag{2.7}$$

Thus by Fourier Transform considerations of Eq. 2.4, one obtains:

$$I(\omega_x,\omega_y) = A\left[O(\omega_x,\omega_y)\ S(\omega_x,\omega_y)\right] \tag{2.8}$$

where x,y are the cartesian co-ordinates in the image plane and (ω_x,ω_y) are the spatial frequencies having dimensions of reciprocal length. $S(\omega_x,\omega_y)$ is the "spread" function which represents the light distribution of a point object. It is merely the impulsive response of the system and hence analogous to the kernal of an electrical network.

To illustrate the above discussion, one might consider a sinusoidal intensity variation in the object plane which is inclined at an angle θ with the x-axis (Fig. 2.3). In this example the following properties of the optical system will be shown:

1. The image intensity distribution varies sinusoidally;
2. The above distribution is of the same spectral frequency;
3. The amplitude and phase of the distribution are dependent upon the spread function of the lens.

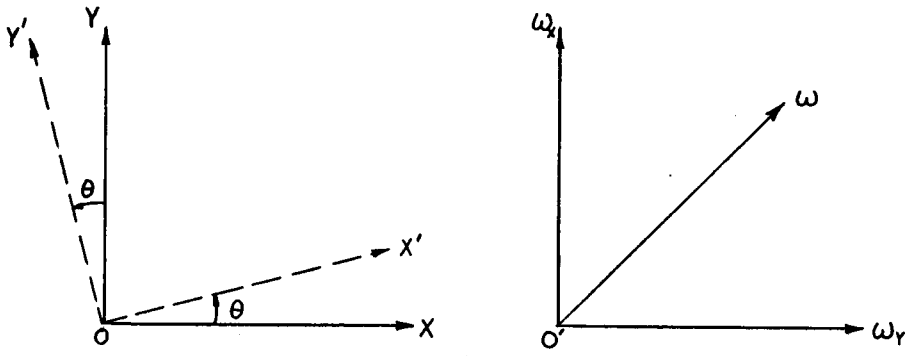

Fig. 2.3. The Cartesian and Spacial Coordinate Systems.

Now, one may write:

$$O(x,y') = Ke^{i\omega_o x} \; ; \tag{2.9}$$

where $\omega_o = \frac{2\pi}{L}$ and L is a unit of length that corresponds to the repetition of the sinusoidal variation that is considered and K is a constant.

But from a transformation of the coordinate system one has:

$$\begin{aligned} x' &= x\cos\theta + y\sin\theta \; , \\ y' &= -x\sin\theta + y\cos\theta \; . \end{aligned} \tag{2.10}$$

Thus substituting Eq. 2.10 in Eq. 2.9 one obtains:

$$O(x,y) = K e^{i\omega_o (x\cos\theta + y\sin\theta)} . \tag{2.11}$$

Again Eq. 2.11 may be written as:

$$O(x,y) = Ke^{i\vec{\omega}_o \cdot \vec{r}} \; ; \tag{2.12}$$

where $\vec{\omega}_o \cdot \vec{r} = \omega_{ox} x + \omega_{oy} y$.

Then

$$i(x,y) = \frac{1}{2\pi} \iint_{-\infty}^{\infty} I(\omega_x, \omega_y) e^{i\vec{\omega}_o \cdot \vec{r}} d\omega_x d\omega_y \; , \tag{2.13}$$

or

$$i(x,y) = \frac{1}{2\pi} \iint_{-\infty}^{\infty} \tau(\omega_x, \omega_y)\, O(\omega_x, \omega_y)\, e^{i\vec{\omega}_o \cdot \vec{r}}\, d\omega_x\, d\omega_y \,, \tag{2.14}$$

where $\tau(\omega_x, \omega_y)$ is the transform of the spread function $\tau(x,y)$ of the lens.

Again from Eq. 2.11 one may show that

$$O(\omega_x, \omega_y) = \frac{K}{2\pi} \iint_{-\infty}^{\infty} e^{i[(\omega_x - \omega_{ox})x + (\omega_y - \omega_{oy})y]}\, dx\, dy \,. \tag{2.15}$$

Thus

$$O(\omega_x, \omega_y) = 2\pi K\, \delta(\omega_x - \omega_{ox})\, \delta(\omega_y - \omega_{oy}) \,. \tag{2.16}$$

Substituting for $O(\omega_x, \omega_y)$ in Eq. 2.14 one obtains:

$$\begin{aligned} i(x,y) &= K \iint_{-\infty}^{\infty} [\delta(\omega_x - \omega_{ox})\, \delta(\omega_y - \omega_{oy})]\, \tau(\omega_x, \omega_y)\, e^{i\vec{\omega}_o \cdot \vec{r}}\, d\omega_x\, d\omega_y \\ &= K\, \tau(\omega_{ox}, \omega_{oy})\, e^{i\vec{\omega}_o \cdot \vec{r}} \end{aligned} \tag{2.17}$$

If $\tau = |\tau| e^{-i\phi}$, then,

$$i(x,y) = K|\tau|\, e^{i(\vec{\omega}_o \cdot \vec{r} - \phi)} = |\tau| e^{-i\phi} O(x,y) \,. \tag{2.18}$$

Again using Eq. 2.13 and 2.16 it follows that

$$i(x,y) = |\tau| K e^{-i(\vec{\omega}_o \cdot \vec{r} - \phi)} = |\tau| e^{-i\phi} O(x,y). \tag{2.19}$$

Thus the properties listed in the beginning of the example have been proved. This leads one to conclude that the lens merely behaves analogously to a linear electrical low-pass filter. Its spectral response is determined by the function

that weights the intensity in the object plane which happens to be the photographic plane in this case. This leads one to explain the behavior of the photographic process.

As mentioned earlier, the approach suggested by Felgett will be considered to describe the properties of the photographic process. Signal to noise ratio concepts are associated with this process. This follows from the fact that when a photographic record is measured in a microphotometer, the resultant wave does possess a certain signal-to-noise ratio. Here, τ , represents a distance variable rather than that of time as in the radar experiment. In particular it represents the position of the origin of the slit. Thus the total transmission when the origin of the slit is at position, τ , is:

$$P(\tau) = k\,p(\tau)\; e^{\frac{2}{N}\int_{-\infty}^{\infty} W(t)\, S(t-\tau)\, dt} , \qquad (2.20)$$

or,

$$\log_e P(\tau) = \log_e [k\,p(\tau)] + \frac{2}{N}\int_{-\infty}^{\infty} W(t)\, S(t-\tau)\, dt \; ; \qquad (2.21)$$

where

k = a normalizing constant,

N = mean square noise fluctuation,

P (τ)= a priori probability of transmission when corresponding to the origin of the slit at, τ ,

S = transmission function of the slit,

W = transmission function of the plate.

The correspondence in the radar and photographic systems is suggested by the respective convolution integrals given in Eq. 2.22. Further, Felgett has also shown that the properties

of the grain can be described almost completely by the autocorrelation function of the developed emulsion.

Now, it may be pointed out that generally in the radar experiment, the frequency composition of the pulse-to-pulse fluctuations at a particular time delay in the received signal is of interest. This information is contained in the power spectrum of these fluctuations. The most practical method of obtaining the power spectrum involves first determining the autocorrelation function of the fluctuations and then taking the Fourier Transform of the same. The power spectrum of the variations in the envelope of the signal after square-law detection has been called a variance spectrum by Welch[7]. It is a measure of the extent of fluctuations of the power about its mean value.

Again, in the photographic experiment one can determine the spectrum of a picture by first obtaining the autocorrelation function of the picture and then taking its Fourier Transform. The spectrum so obtained is analogous to a power spectrum of a signal in communication theory[8].

Thus this manner of viewing the radar and photographic systems leads one to investigate possibilities of correlation

---

[7]Welch, P.D. "Interpretation and Prediction of Radar Terrain Return Fading Spectra" New Mex. A&M Phys. Sc. Lab. Rept. AER-14-W. May 1955.

[8]Elias, P. "Optics and Communication Theory" Jour. of the Optical Soc. of America, Vol. 43, No. 4, April 1953, pp. 229-332.

between the variance and power spectrums respectively of the two systems. A detailed account of the manner in which this study has been done will now be considered.

The Variance Spectrum

The radar experiment was so designed that a narrow pulse type radar with the antenna oriented vertically was flown in a straight level path with a constant velocity over a relatively homogenous terrain. From this record a time series was obtained by reading values of the power return at a fixed time delay in the received pulse.

The autocorrelation function may be written as:

$$\eta(\tau) = \left\langle [p(t) - \overline{p(t)}][p(t+\tau) - \overline{p(t)}] \right\rangle \; ; \qquad (2.22)$$

where $p(t)$ is the power of the return pulse at delay time, . Further, the time series obtained in the manner indicated above was assumed to be stationary. This permits one to consider the variance spectrum to be the Fourier Transform of the autocorrelation function. Thus, it follows from Eq. 2.22 that

$$V(\omega) = 2\int_{o}^{\infty} \eta(\tau) \cos \omega t \, dt \qquad (2.23)$$

Since radar data is a representation of a sampled data the variance spectrum is valid for an upper limit frequency (i.e., the Nyquist frequency) given by

$$F_u = \frac{1}{2\,\Delta t} \; ;$$

where Δt is the sampling interval.

An estimator was chosen to determine the autocorrelation function. This was of the form

$$R_k = \frac{1}{N-K} \sum_{i=0}^{N-K-1} [(x_i - \bar{x})(x_{i+K} - \bar{x})] \tag{2.24}$$

where $k = 0,1,2,\text{----} m$,

and where x is the sample power return, $\bar{x}$ is an average over the population and m is the largest lag for which the autocorrelation function is computed. Thus if $\psi(\tau)$ (Fig. 2.5) represents a continuous function from which the R_k values are samples, then an estimate of the complex power spectrum is given by

$$q'(\omega) = 2\int_0^{\infty} \psi(\tau) \cos \omega\tau \, d\tau \tag{2.25}$$

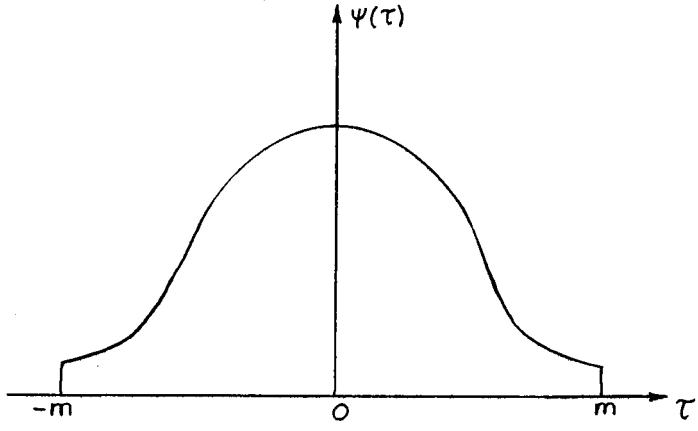

Fig. 2.5. A Function From Which Values of R_k are Sampled.

Now, $\psi(\tau)$ is equivalent to the product of the desired autocorrelation function $\eta(\tau)$ and a product function $\phi(\tau)$ which is defined by

$$\phi(\tau) = \frac{1}{2}\left(1 + \cos\frac{\pi}{m}\tau\right) , \text{ for } |\tau| < m , \tag{2.26}$$

and $\quad = 0$ otherwise.

The choice of the product function given by Eq. 2.26 is considered appropriate since the corresponding window has very small side lobes so that adjacent frequencies will have little effect on the spectrum[9].

Therefore Eq. 2.25 may be written:

$$q'(\omega) = 2\int_0^\infty \eta(\tau)\,\phi(\tau)\cos\omega\tau\,d\tau\,, \qquad (2.27)$$

$$= \int_{-\infty}^{\infty} p'(\mu)\,r'(\omega-\mu)\,d\mu\,,$$

where,

$$r'(\omega) = 2\int_0^\infty \phi(\tau)\cos\omega\tau\,d\tau\,. \qquad (2.28)$$

From Eq. 2.27 it follows that the spectrum estimate is the convolution of the desired spectrum with the spectrum of the product function $\varphi(\tau)$.

The variance spectrum is given in terms of a frequency unit called the yule. The yule is defined as equal to $\frac{\pi}{m}$ radians per sampling interval. On substituting for the product function $\varphi(\tau)$ in Eq. 2.27 one may obtain an expression for the variance spectrum which can be evaluated by numerical means. This expression is

$$q'(y) = \Delta\tau\left[R_o\phi_o + 2\sum_{i=1}^{m-1} R_i\phi_i\cos\left(\tfrac{\pi}{m}y\cdot i\right) + R_m\phi_m\cos\pi y\right]\,; \qquad (2.29)$$

where $y = \frac{\pi}{m}$ radians per sampling period, so that the argument

[9] Blackman, R.B. and Tukey, J.W. "The Measurement of Power Spectra" Dover Publications Inc. 1958, pp 14-15.

of the cosine is $\omega\Delta t_i = \frac{\pi}{m} y_i$. Thus by means of Eq. 2.29, the variance spectrum may be plotted with respect to the frequency in yules.

The Power Spectrum of the Photographic Experiment

The development of an expression to compute the power spectrum is similar to that outlined for the variance spectrum of the radar experiment. The portion of this discussion that concerns the measurement of the autocorrelation function of a transparency is based on a method suggested by Kretzmer[10].

Here the time variable, τ, is replaced by the space co-ordinate, $l\angle\theta$, and the correlation time shift, τ, is replaced by the space shift l. Thus the expression for the autocorrelation function may be written:

$$A(l\angle\theta) = \langle T(l\angle\theta)\, T(l\angle\theta + \Delta l\angle\theta) \rangle \; ; \qquad (2.30)$$

where $T(l\angle\theta)$ is the optical transmission which is a function of two dimensional space expressable in polar coordinates.

The space domain autocorrelation is easier to measure experimentally than that of the time domain. This is a result of the fact that it involves merely measureing the relative optical transmission of two identical cascaded transparencies shifted from register by a variable amount. In accordance with the principle of maximum power transfer, the transmission is always a maximum when the two slides are in precise register

[10] Kretzmer, E.R. "Statistics of Television Signals" Bell System Technical Journal, Vol. 31, July 1952, pp. 751-763.

which corresponds to $\Delta l = 0$. In such a measurement the averaging process is inherent.

Now, transmission is defined:

$$T(l\angle\theta) = \frac{R_2(l\angle\theta)}{R_0(l\angle\theta)} \quad ; \tag{2.31}$$

where $R_2(l\angle\theta)$ is the response of the photomultiplier tube with two cascaded transparencies, with one of them shifted by an amount, l , with respect to the other and $R_0(l\angle\theta)$ the corresponding response with no transparancies. θ is the angle the line of flight makes with the horizontal.

Thus the autocorrelation function may be expressed:

$$A(l\angle\theta) = \frac{T_2(l\angle\theta)}{T_2(0\angle\theta)} \quad ; \tag{2.32}$$

where $T_2(l\angle\theta)$ is the transmission through two cascaded transparencies with one of them shifted through a distance, l , with respect to the other and $T_2(0\angle\theta)$ the transmission when they are in precise register. θ is again the angle the line of flight makes with the horizontal.

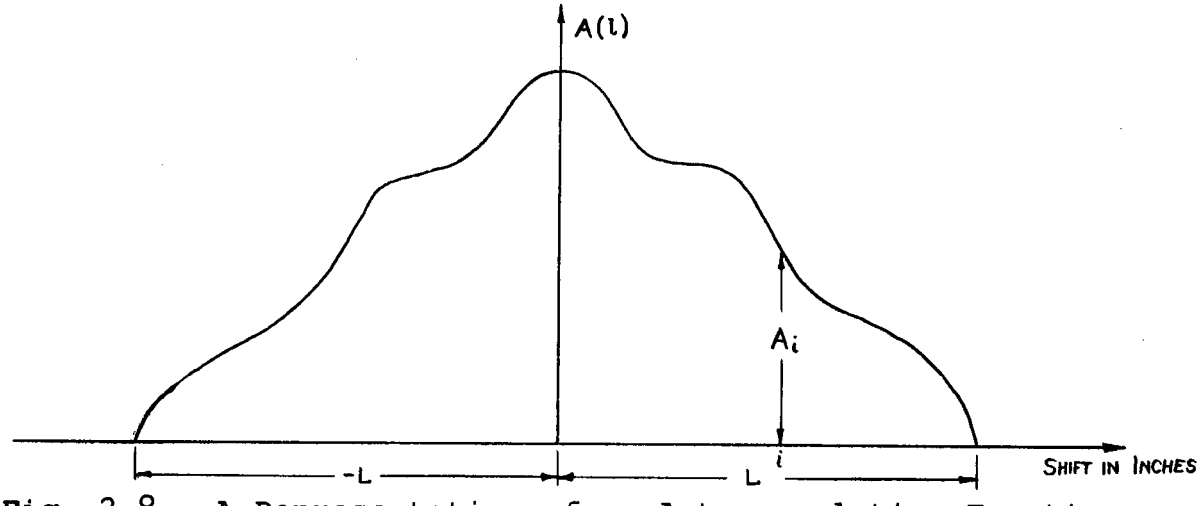

Fig. 2.8. A Representation of an Autocorrelation Function of a Transparency.

Fig. 2.8 may be considered to represent an autocorrelation function determined from a photographic experiment. The estimate of $A(l)$ may be referred to as $A'(l)$. Then,

$$A'(l) = \sum_{i=1}^{m} A_i \left(i \frac{L}{m}\right) + A_0(0)$$

where m is the total number of equal intervals the total shift L is divided into. The value of m corresponds to the largest lag in the radar experiment.

The product function chosen is of the form:

$$\phi(l) = \frac{1}{2}\left(1 + \cos\frac{\pi}{m} l\right), \quad \text{for } |l| < m, \tag{2.33}$$

and = 0 otherwise.

The desired power spectrum may be expressed:

$$Q'(\omega) = 2\int_0^{\infty} A(l)\,\phi(l)\cos\omega l\, dl\,. \tag{2.34}$$

The yule is again used as the unit of frequency and defined as equal to $\frac{\pi}{m}$ radians per shift, where m is the total number of shifts. Thus on substituting for $\varphi(l)$ (Eq. 2.27) in Eq.2.28 the power spectrum is expressed:

$$Q'(y) = \Delta l \left[A_0\phi_0 + 2\sum_{i=1}^{m-1} A_i\phi_i \cos\left(\frac{\pi}{m} iy\right) + A_m\phi_m \cos\pi y\right]; \tag{2.35}$$

where $y = \frac{\pi}{m}$ radians per shift so that the argument of the cosine form is $\omega\Delta l.i = \left(\frac{\pi}{m}\right)yi$. The power spectrum may now be computed and then compared with the variance spectrum of the radar experiment.

CHAPTER III

A PROCEDURE TO LOCATE PORTIONS OF A PHOTOGRAPH THAT CORRESPOND TO ZONES OF THE TERRAIN ILLUMINATED BY RADAR

The basic problem encountered in correlation studies is the location of portions of a photograph that correspond to zones of the terrain illuminated by the radar. The autocorrelation function of the photographic data can then be determined experimentally by working with this portion of the photograph. A procedure to accomplish this will now be developed on the basis that the parameters given in Table 3.1 are known.

TABLE 3.1

Parameter	Symbol
Sampling rate as read on film	n
Number of samples read	N
Pulse repetition rate	k
Ground Speed of Aircraft	R feet per sec.
Distance along the line of flight corresponding to the duration of recording radar data - i.e. distance on photograph between ground return camera points.	ℓ cms

The procedure will be discussed in two stages. The first of these consists in determining the scale of the photograph which enables one to locate any pulse of the radar experiment on the photograph. This is followed by the second stage which concerns the determination of the radial limits of a zone corresponding to a pulse that has been located on the photograph.

Determination of the Scale of a Photograph

The scale of a photograph can be expressed in terms of the characteristics given in Table 3.1. It follows that the total number of pulses considered to analyze the radar data is nN. Thus, the duration of recording radar data = $\frac{nN}{l}$ seconds. Again, the distance tranversed along the terrain while recording radar data = $(\frac{nN}{l} \cdot R)$ feet.

Hence, the scale of the photograph is expressed:

$$S = \frac{NnR}{l} \text{ feet per cm.}$$

Alternately, this scale may also be expressed:

$$S' = \frac{Nn}{l} \text{ pulses per cm.} \qquad (3.1)$$

Determination of the Radial Limits for a Given Zone

A method to determine the radial limits for a given zone may be explained with the aid of Figs. 3.1 and 3.2. Fig. 3.1 represents a typical transmitted and returned pulse $P(d)$ plotted with respect to the time delay d. The duration of the transmitted pulses is τ and the time interval between them is T. The geometry of reradiation of a pulse of width τ from the terrain is shown in Fig. 3.2.

The portion of the returned power at delay d that is caused by the leading edge of the transmitted pulse has traveled through a distance $2R_o$ at velocity c. Thus

$$R_o = h + \frac{cd}{2} \quad , \quad (d > 0) \quad ,$$

and the returned pulse does not exist for $d \leq 0$.

Similarly, the portion of the returned power at delay d that

is caused by the trailing edge of the transmitted pulse has traveled $d + \frac{2h}{c} - \tau$ seconds (Fig. 3.1) through a distance $2R_i$ at a velocity c.

Thus,

$$Ri = h + \frac{c(d - \tau)}{2} \quad , \quad (d - \tau > 0) \quad . \tag{3.2}$$

For $d - \tau \leq 0$, R_i is equal to h and the annulus then becomes a circle.

Again, the annular region, ΔA, (Fig. 3.2) that yields the power, $P(d_1)$, at a fixed delay, d_1, may be defined by the outer and inner angles that are given by:

$$\cos\theta_o = \frac{h}{R_o} \quad , \tag{3.3}$$

$$\cos\theta_i = \frac{h}{R_i} \quad . \tag{3.4}$$

Having determined R_o and R_i, one may obtain r_o and r_i and these may be located on the photograph with the help of the scale of the photograph. This technique is employed to analyze some of the photographic data that has been used for correlation studies.

Two examples are considered. The symbols used in these examples have been given in Table 3.1.

Example 3.1

Radar data obtained from film or run No. 37-30L (Appendix, Table A.3) has the following parameters:

nN = 3765
k = 200 pps
R = 64 meters per sec. or 209.97 feet per sec.
l = 4.45 cms.

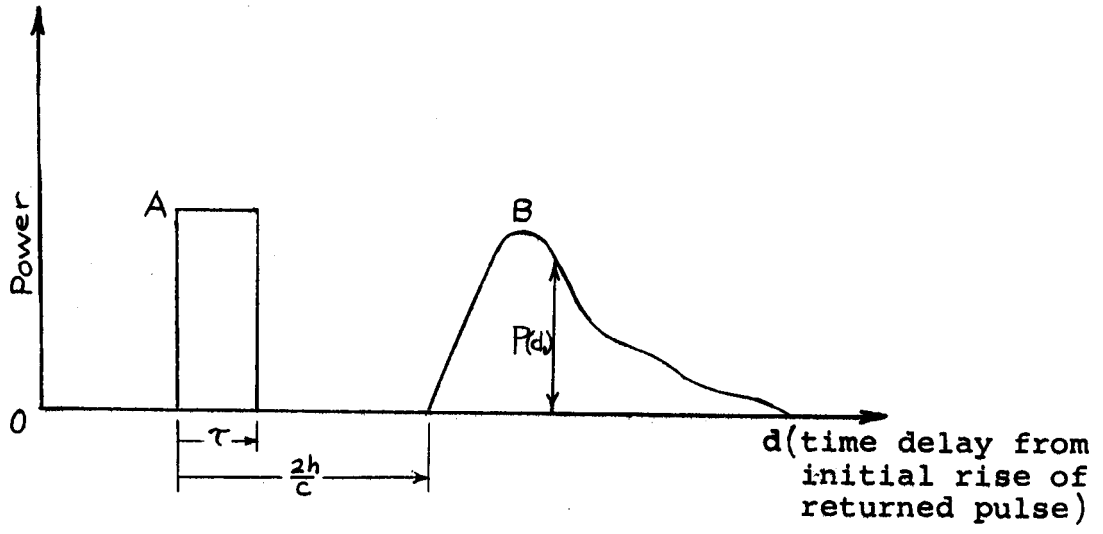

A. Transmitted pulse
B. Returned pulse
τ. Pulse width
h. Altitude of aircraft
c. Velocity of light
d. Time delay from initial rise of returned pulse.
d_1.A fixed time delay
$P(d_1)$. Power level of returned pulse at fixed delay d_1.

Fig. 3.1 A typical transmitted and returned pulse.

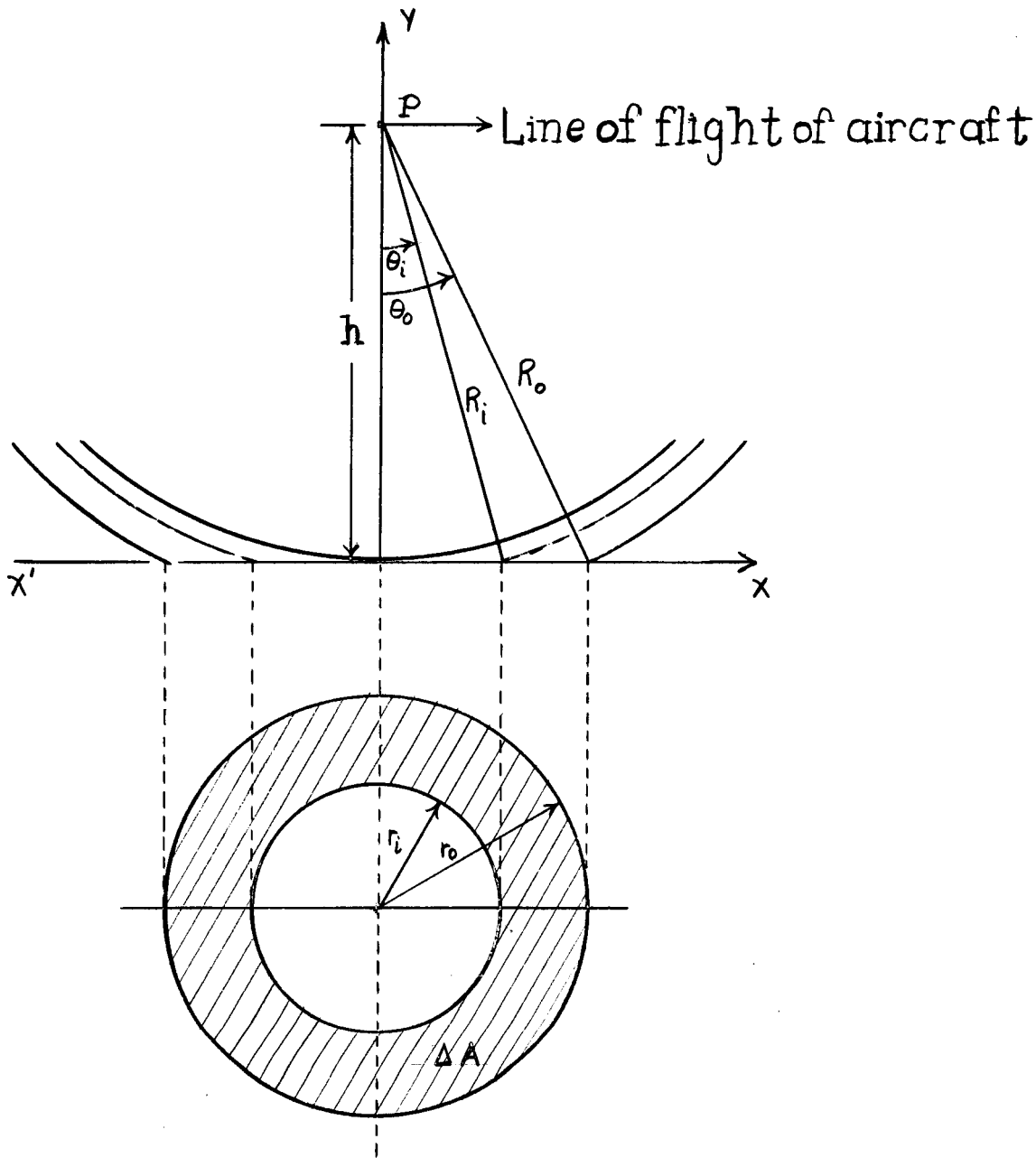

P - Position of aircraft and radar.

d - Time delay of returned pulse.

ΔA - Annular region corresponding to Zone 1.

R_o, R_i - Outer and inner ranges that define the active annular region corresponding to Zone 1.

r_o, r_i - Radial limits of Zone 1.

Fig. 3.2. The Geometry of a Reflected Pulse of Width from the Terrain.

Fig. 3.3 is an aerial photograph of the terrain with the line of flight indicated on it. From report No. PSL 37-30L (Appendix, Table A.3) one may obtain Table 3.2.

TABLE 3.2

h = altitude of aircraft = 3877 feet

Zone 1	Radial Limits	Angular Limits
1	0 - 770 feet	0 - 11.2°
2	944 - 1144 feet	13.7 - 16.4°
3	1340 - 1492 feet	19.1 - 21.0°

It is required to locate the zones on the photograph that correspond to the radar experiment. The radial limits of Zone 1 have been shown in Fig. 3.4.

Solution

The scale of the photograph may be computed from Eq. 3.1 as:

$$S = \frac{NnR}{lk} = \frac{3765 \times 209.97}{4.45 \times 200} = 889 \text{ feet per cm.} \qquad (3.5)$$

or,

$$S' = \frac{Nn}{l} = \frac{3765}{4.45} = 846 \text{ pulses per cm.} \qquad (3.6)$$

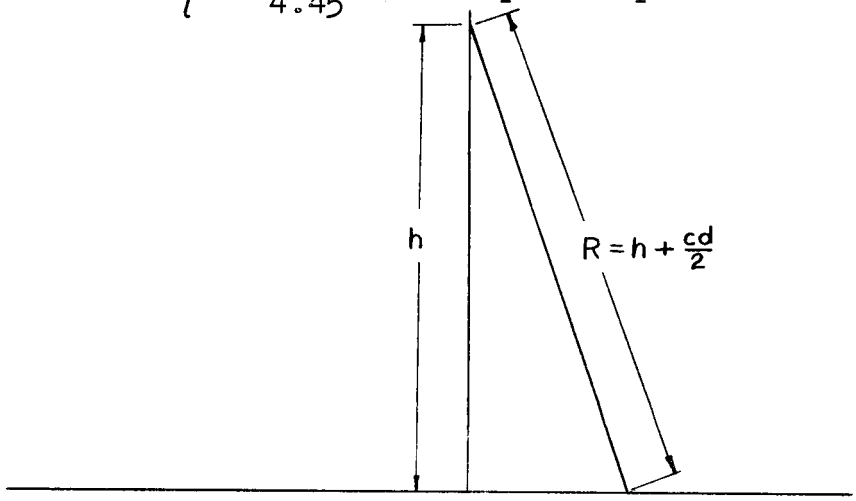

Fig. 3.4. Radial Limits for Zone 1 of Example 3.1

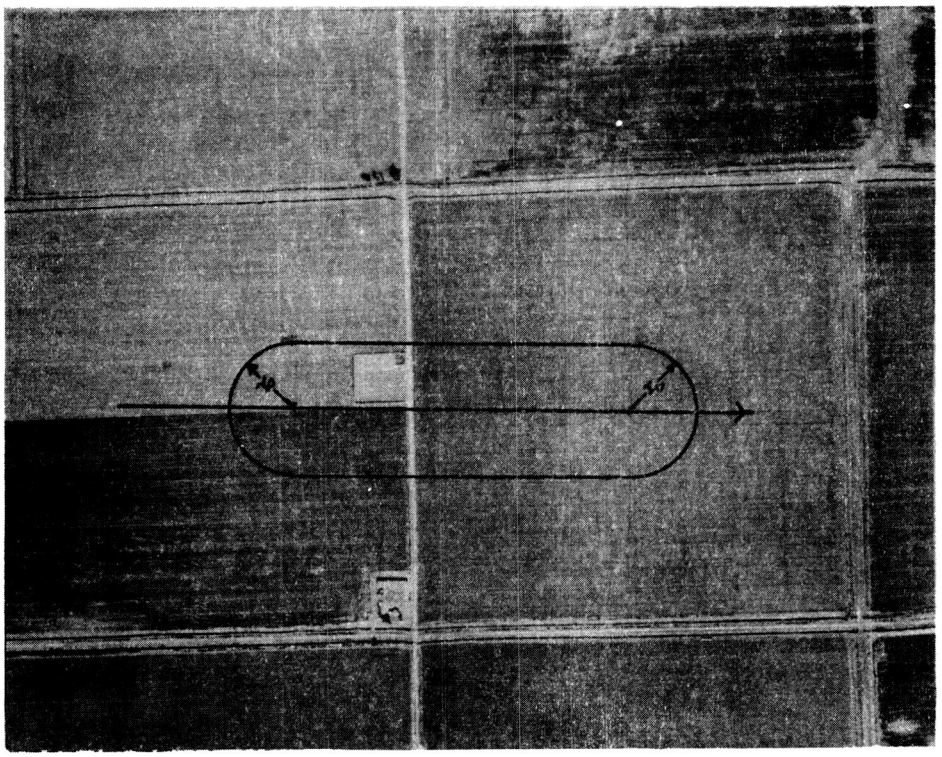

Fig. 3.3. An Aerial Photograph of a Farmland with the Line of Flight and the Area Corresponding to Zone 1 Located on it.

From Fig. 3.4 one obtains:

$$\tan\theta = \frac{r}{h} = \tan 11.2^{\circ} = 0.198 \quad ;$$

i.e. $$r = 767.7 \text{ feet} = \frac{767.7}{S} = \frac{767.7}{889} = 0.885 \text{ cm.}$$

Further, any pulse, i, may be located on the photograph by merely measuring $\frac{i}{S'}$ cms. from the point of commencement of the ground return camera run.

However, for the autocorrelation experiment, the pulses that correspond to the commencement and end of the ground return camera run need be located. The region they enclose between them (shown in Fig. 3.3) represents that portion of the terrain that is responsible for the radar data obtained from zone 1.

Example 3.2

Film or run No. 32-29L (Appendix, Table A.3) has the following parameters:

$N = 474$
$n = 6$
$k = 195$ pps
$R = 60$ meters per sec. or 196.85 feet per sec.
$l = 3.92$ cms.

An aerial photograph of the terrain is given in Fig. 3.5 and the line of flight has been shown on it. From report No. PSL 32-29L (Appendix, Table A.3) one may obtain Table 3.3.

TABLE 3.3

h = altitude of aircraft = 3919 feet

Zone 1	Radial Limits	Angular Limits
1	0 - 786 feet	0 - 12°

Fig. 3.5. An Aerial Photograph of a Residential Area with the Line of Flight and the Area Corresponding to Zone 1 Located on it.

It is also stated that only Zone 1 was considered and that the same was divided into two parts (parts a and b) while analyzing the radar data of this experiment. The radial limits that correspond to parts, a, and, b, of Zone 1 are shown in Fig. 3.6.

Solution

Using Eq. 3.1 one may obtain the scale of the photograph to be

$$S = \frac{NnR}{lk} = \frac{474 \times 6 \times 196.85}{3.92 \times 195} = 732 \text{ feet per cm.;} \quad (3.7)$$

or,

$$S' = \frac{Nn}{l} = \frac{474 \times 6}{3.92} = 725 \text{ pulses per cm.} \quad (3.8)$$

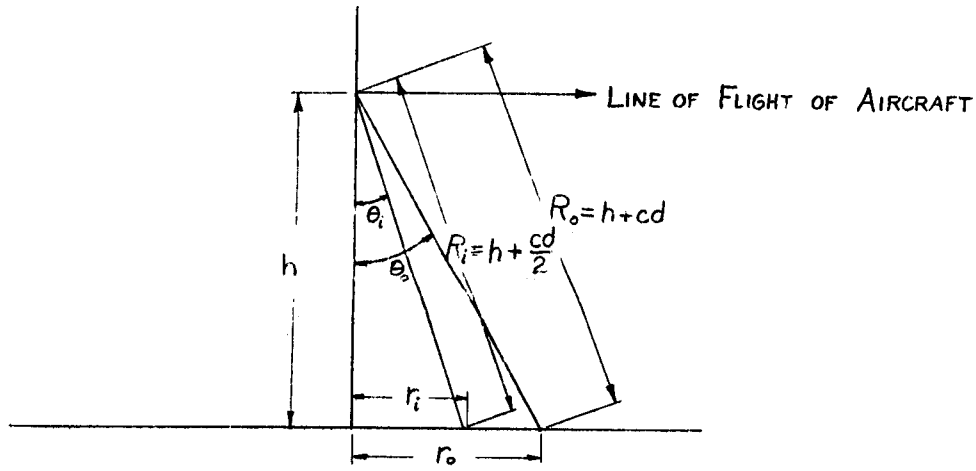

Fig. 3.6. Radial Limits of Zone 1 of Example 3.2.

From Fig. 3.6 it follows that:

$$\cos\theta_o = \frac{1}{1 + \frac{cd}{2h}} \quad ; \quad (3.9)$$

where $\theta_o = 12^o$,

$h = 3703$ feet or 1129 meters,

$c = 300$ m/micro-sec.,

d = time delay in micro-sec.

$\tau = 0.1$ micro-sec.

On substituting these values in Eq. 3.5 one obtains

$$d = 0.168 \text{ micro-sec.}$$

Again, $\cos\theta_i = \dfrac{1}{1 + \dfrac{c(d - \tau)}{2h}}$, where τ is the pulse width.

For

$h = 1129$ meters,

$c = 300$ m/micro-sec.,

$d = 0.168$ micro-sec.,

and $\tau = 0.1$ micro-sec. one obtains

$$\cos\theta_i = 0.99104$$

But $\cos\theta_i = \dfrac{h}{R_i}$

Thus $R_i = 1139$ meters.

Similarly from $\cos\theta_o = \dfrac{h}{R_o}$, it may be shown that $R_o = 1154.2$ meters. Thus it follows from Fig. 3.6 that $r_o = (1154.2^2 - 1129^2)^{1/2} = 238.6$ meters, or 782.8 feet. On the photograph $r_o = \dfrac{782.8}{S} = \dfrac{782.8}{732} = 1.07$ cm. In a similar manner it may be shown that $r_i = 485.55$ feet. Thus on the photograph r_i measures $\dfrac{485.55}{S} = \dfrac{485.55}{732} = 0.66$ cm. As in the previous example any pulse, i, may be located on the photograph by merely measuring $\dfrac{i}{S}$, cms. from the point of commencement of the ground return camera run.

Again, the area which is to be used for the autocorrelation experiment is that which is enclosed between the pulses that correspond to the commencement and end of the ground return camera run. This area has been shown in Fig. 3.5.

CHAPTER IV

DESIGN OF EXPERIMENT AND EXPERIMENTAL PROCEDURE

Equipment

The picture autocorrelator is shown in Figs. 4.1, 4.3, and 4.4. Fig. 4.1 shows a cross-sectional view while Figs. 4.3 and 4.4 respectively show the general set up and close-up view of the transparency holding and shifting mechanism.

The chamber at the top contains a light source which is connected to a d-c battery which provides light of constant intensity. A is a collimating lens while the lens system, B and C, serve as a condensing device.

The two transparencies to be used in an autocorrelation experiment may be mounted below the collimating lens A. One of the transparencies is fixed whereas the other is mounted on a movable rectangular frame. This frame is moved by means of a micrometer. The micrometer is capable of registering shifts of the order of 0.001 inch.

The light that emerges from the transparencies is focused on one face of a ground glass. Diffused light emerges from the other face of the ground glass and is collected by a photomultiplier tube. The circuitry associated with the tube is shown in Fig.4.2. A well regulated power supply is used to provide the appropriate plate voltage to the photomultiplier tube. The output of the tube is registered on a microammeter connected as shown in Fig. 4.2.

Prior to recording data pertinent to the autocorrelation experiment the apparatus is calibrated. Calibration tests

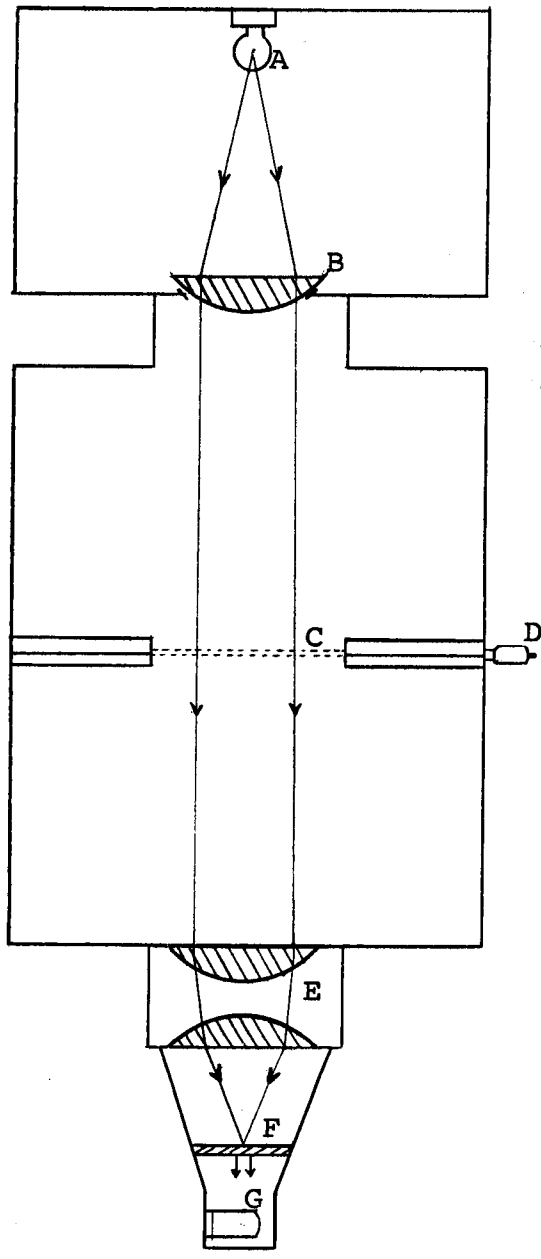

A: Light Source
B: Collimating lens
C: Transparencies
D: Micrometer
E: Condensing lens
F: Ground Glass
G: Photomultiplier tube

Fig. 4.1. A Cross-Sectional View of the Picture Autocorrelator.

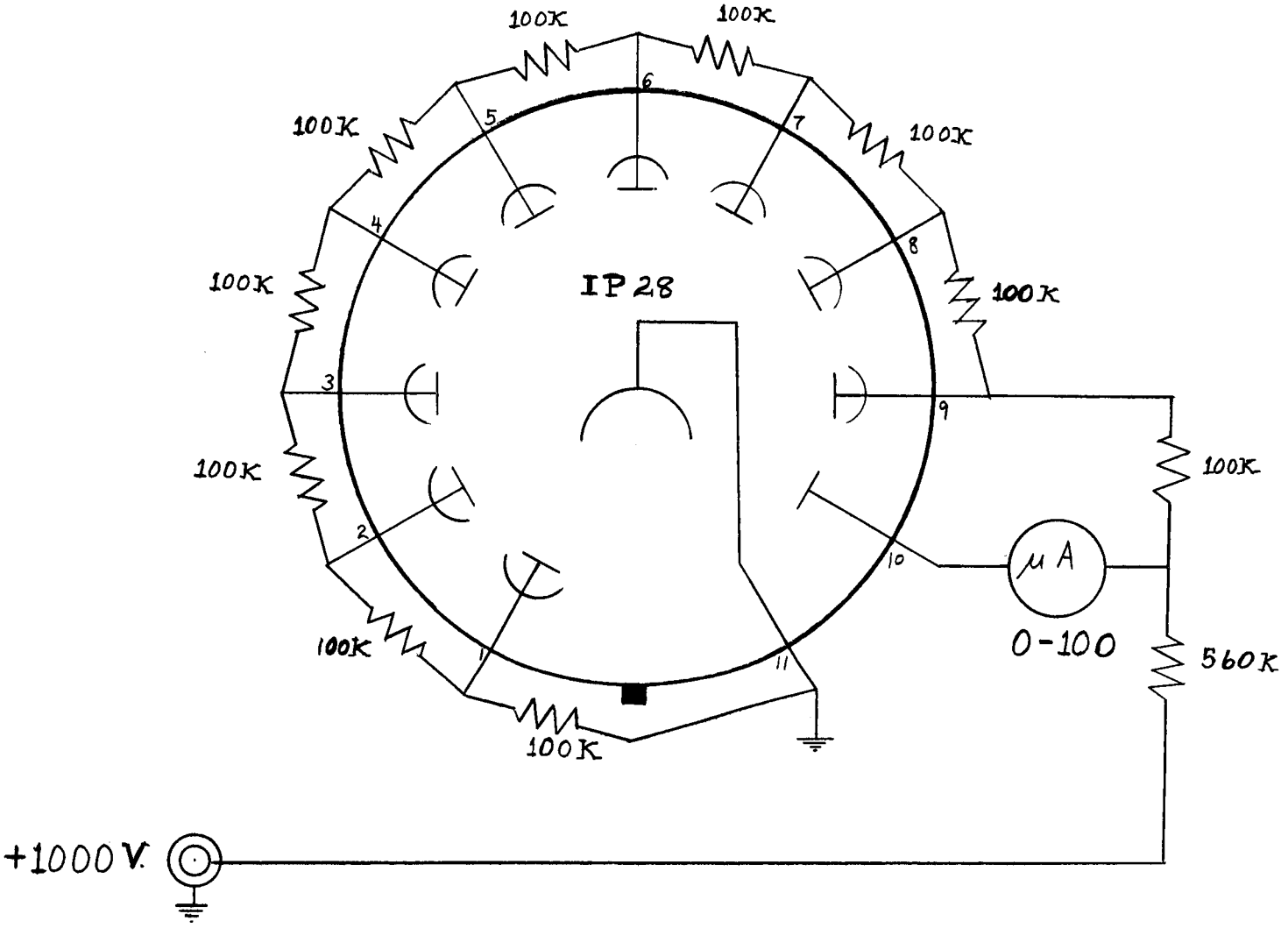

Fig. 4.2. Circuit Diagram of the Photomultiplier Tube.

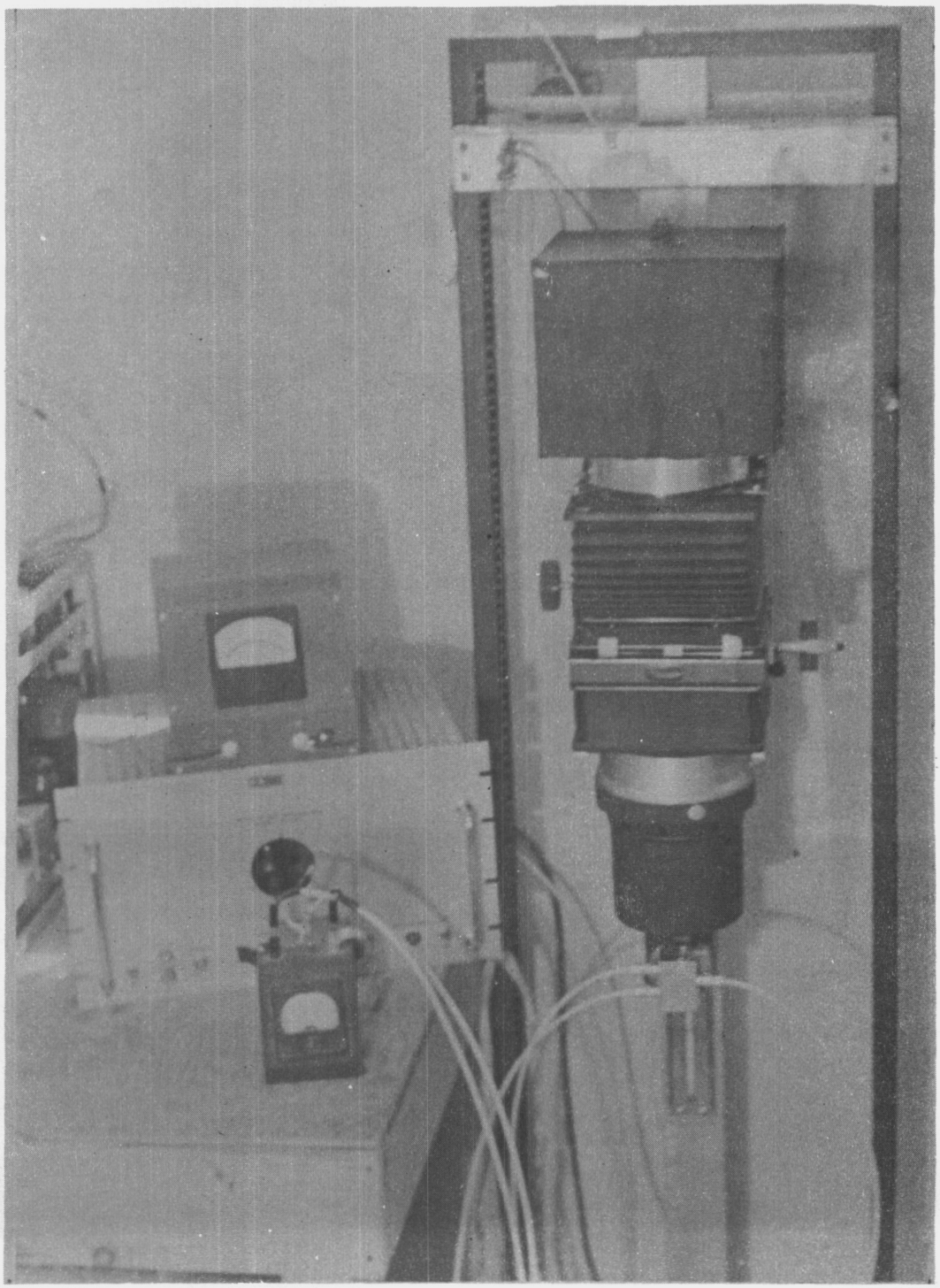

Fig. 4.3. General Set Up of the Picture Autocorrelator

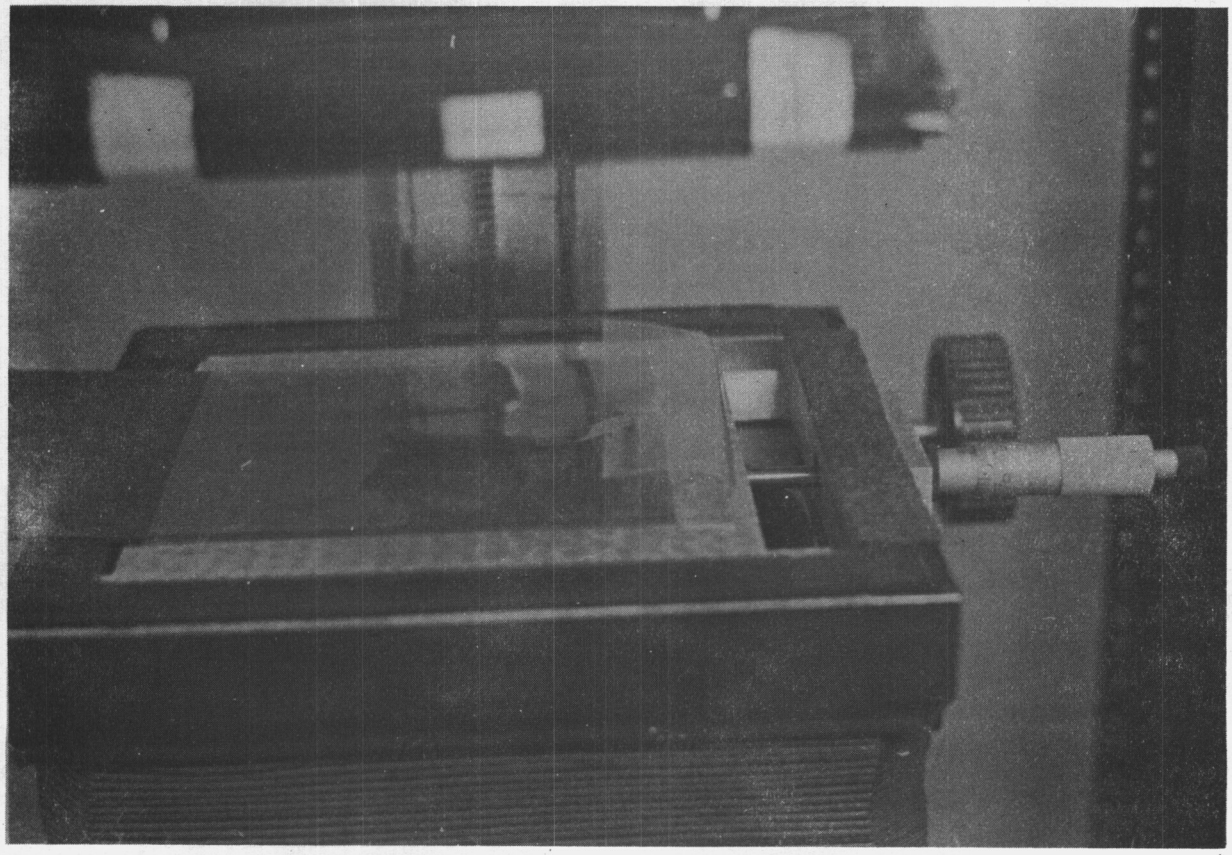

Fig. 4.4. A Close Up View of the Holding and Shifting Mechanism of the Picture Correlator.

are conducted in order to check for the following characteristics of the system:

1. Fatigue of the photomultiplier tube.
2. Linearity of the photomultiplier tube.
3. Stability of the voltage to the light source.

The photomultiplier tube is tested for fatigue by recording the response of the tube with respect to an aperture size of one inch diameter at the rated voltage. The reading so obtained is then compared with the response of the tube to similar tests which were conducted prior to former autocorrelation experiments.

In order to test for the linearity of the photomultiplier tube, apertures of size 1/4, 1/2, 3/4, and 1 inch diameter are used and the corresponding responses of the tube are recorded. Now, the quantity of light flux incident on the photomultiplier tube varies as the area of the aperture. Thus a plot of the response of the tube corresponding to these apertures versus d^2/D^2 is considered, where, d, is the diameter of the smallest aperture and, D, is the diameter of each of the larger apertures. A typical plot obtained from such a calibration process is shown in Fig. 4.5.

The stability of the voltage to the light source is easily checked by measuring the specific gravity of the d-c battery. This reading is compared with a reference value of 1250. This procedure thus ensures a constant voltage to the light source and hence the quantity of light flux incident on one face of the transparency is the same for each experiment.

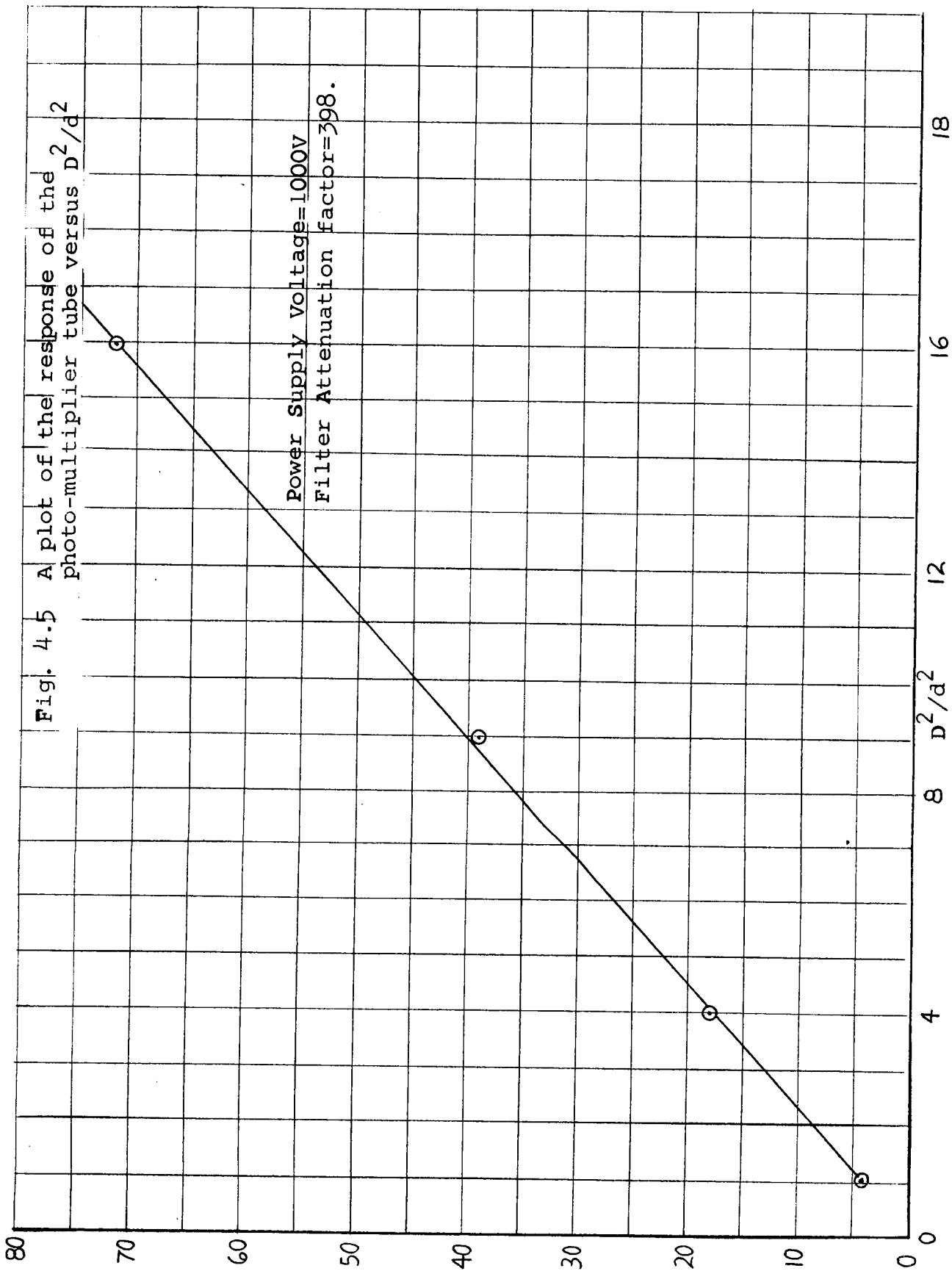

Fig. 4.5 A plot of the response of the photo-multiplier tube versus D^2/d^2

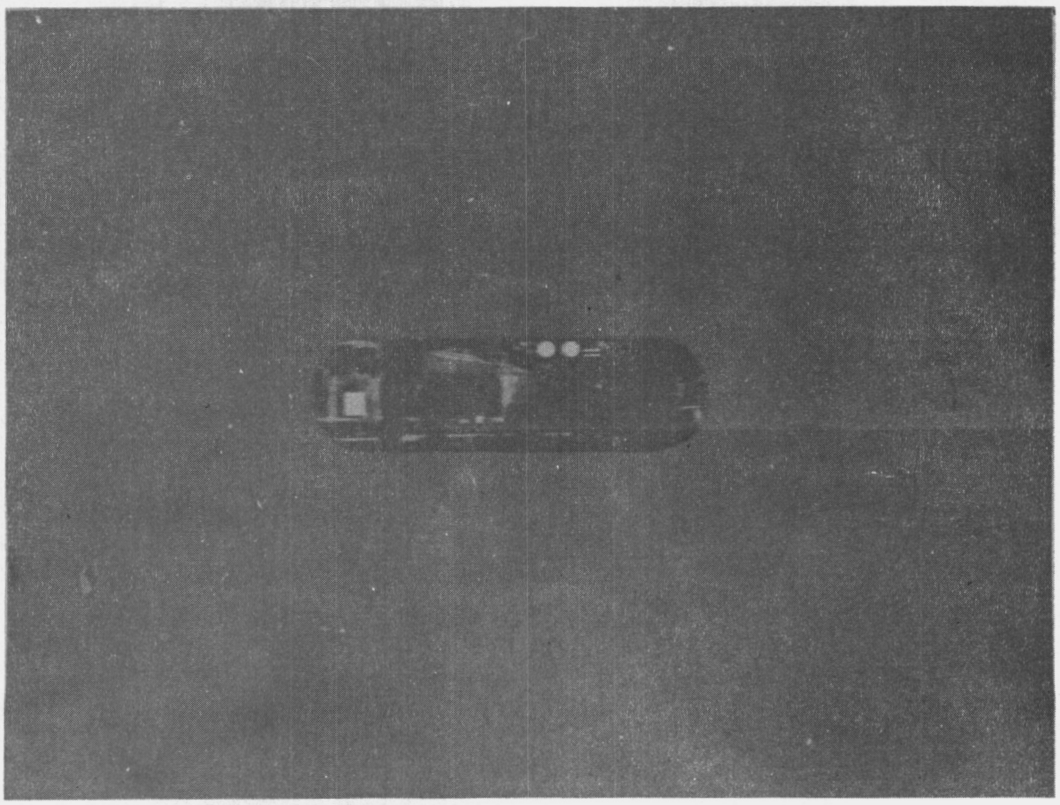

Fig. 4.6. Transparency with the Area Corresponding to Zone 1 Located on it. 41

Experimental Procedure

The aparatus is ready for recording data once the calibration process is complete. The first phase of the experiment consists in locating the portion of the transparency that corresponds to the illuminated portion of the terrain from which the radar data was obtained. This is accomplished by employing the procedure explained in Chapter III. After the area corresponding to Zone 1 has been located the remaining portion of the transparency is masked with black construction paper. Fig. 4.6 shows a transparency with the area corresponding to Zone 1 located on it. In an autocorrelation experiment two identical transparencies with the areas located in this manner are used.

After the zones on the transparencies have been located they are cascaded in position in the autocorrelator so that the line of flight coincides with the axis of the direction of shift which is indicated on the shifting mechanism. As mentioned earlier the shift is registered on a micrometer. It is essential that one transparency be moved with respect to the other along the line of flight as this corresponds to the manner in which the pulsed radar illuminates the terrain when mounted on a moving aircraft.

The transparencies are then brought into precise register by shifting the movable transparency. This position of the transparencies is indicated by a maximum deflection of the microammeter. This reading of the microammeter is recorded. The movable transparency is then shifted in increments of 0.05

inch along the line of flight and the corresponding readings of the microammeter are recorded. This shifting operation is continued till the microammeter reads close to zero. This experiment is repeated for shift against the line of flight and the readings of the microammeter are again recorded. The values so obtained are found to be very close to these obtained while shifting along the line of flight. In other words, the autocorrelation function is an even function. This is to be expected since the two transparencies are identical. However, this procedure gives an indication of the degree of accuracy afforded by the shifting arrangement and the rest of the apparatus.

The next phase of the experiment relates to obtaining the response of the photomultiplier tube with no transparencies. With the aid of these readings the transmission corresponding to the various shifts may be computed.

The transparencies are removed and only the black construction paper masks are cascaded in position in the autocorrelator. As in the previous case the zones are brought in precise register. However, in this case it was found that the photomultiplier tube reached saturation. Thus neutral density optical filters were used to overcome this difficulty. The use of such filters correspondingly introduces an attenuation factor which may be accounted for later. If a filter has n for its series number, then it implies that the corresponding attenuation factor $a = 10^n$, which follows from the relation $n = \log_{10} a$. The experiment is repeated in

a manner similar to that explained with respect to the experiment in which both transparencies were used. The readings of the microammeter thus obtained are recorded.

The relative transmission and hence the autocorrelation function can now be computed. The transmission corresponding to a shift Δl is given by:

$$T(\Delta l) = \frac{\text{microammeter reading at shift } \Delta l \text{ with two transparencies}}{\text{microammeter reading at shift } \Delta l \text{ with no transparencies}}.$$

A plot of shift Δl versus $A(\Delta l)$ yields the desired autocorrelation function, where,

$$A(\Delta l) = \frac{\text{Transmission at shift } \Delta l}{\text{Transmission at zero shift}}.$$

Table 4.1 shows a typical data reduction sheet which was used to obtain the autocorrelation function of a transparency. The autocorrelation function obtained from this set of data is shown in Fig. 4.7.

The Fourier Transform of the autocorrelation function obtained experimentally by the procedure explained in this chapter yields the desired power spectrum. This will be discussed in the following chapter which is related to data reduction and the results.

TABLE 4.1 Film or run #32-26L

Shift	Actual Response with no negatives $\times 10^{-2}$: $R_o(\tau\angle\theta)$ Attenuation Factor = 398	Response with Two Negatives $R_2(\tau\angle\theta)$	Transmission $\times 10^2$ $T(\tau\angle\theta)$	Autocorrelation $A(\tau\angle\theta)$
0	143.28 uA	18.4 uA	.1284	1
.05	139.3	12.75	.09152	.7127
.1	135.32	11.8	.0872	.679
.15	127.36	11.5	.0929	.7031
.2	125.37	10.4	.08295	.6459
.25	123.38	9.8	.07943	.6185
.3	121.39	9.4	.07744	.603
.35	119.4	8.8	.0737	.5739
.4	115.42	8.4	.07278	.5667
.45	111.44	8	.07179	.559
.5	107.46	7.7	.07165	.558
.55	103.48	7.4	.07151	.5568
.6	99.5	7.1	.07135	.5556
.65	95.52	6.75	.07066	.5502
.7	91.54	6.4	.06991	.5444
.75	87.56	5.8	.06624	.5158
.8	81.59	5.4	.06618	.5153
.85	79.6	5.25	.06595	.5135
.9	73.63	5.2	.07062	.5499
.95	69.65	5.2	.07465	.5814
1.0	63.68	4.75	.07459	.5808
1.05	58.9	4.2	.0713	.5552
1.1	53.73	3.8	.07072	.5507
1.15	48.556	3.3	.06796	.5292
1.2	44.178	3.0	.0679	.5287
1.25	39.8	2.9	.07286	.5674
1.3	35.82	2.7	.07537	.5869
1.35	31.84	2.5	.07581	.6114
1.4	27.86	2.25	.08076	.6289
1.45	24.676	2.1	.0851	.6727
1.5	21.89	1.9	.08679	.6758
1.55	18.706	1.8	.09622	.7493
1.6	15.92	1.7	.10678	.8315
1.65	13.93	1.2	.08614	.6729
1.7	11.94	1.0	.08375	.6522
1.75	9.95	0.9	.0945	.7359
1.8	8.358	0.8	.09571	.7453
1.85	7.562	0.6	.07934	.6178
1.9	5.97	0.5	.08375	.6522
1.95	5.174	0.45	.08697	.6772
2.0	3.98	0.3	.07537	.5869
2.05	3.582	0.2	.05583	.4346
2.10	2.388	0.1	.04187	.326
2.15	1.99	0.05	.025125	.163
2.2	1.195	0.025	.01206	.0815
2.25	0.796	0.0125	.00603	.04075
2.3	0.33	0.01	.003	.0204
2.35	0	0	0	0

Fig. 4.7 Autocorrelation of a transparency obtained from data in table 4.1

CHAPTER V

DATA REDUCTION AND RESULTS

The expression for the desired power spectrum of a transparency which was developed in Chapter II (Eq. 2.34) has the form:

$$Q'(\omega) = 2\int_0^{\infty} A'(l)\,\phi(l)\cos\omega l\, dl \;; \qquad (5.1)$$

where $Q'(\omega)$ is the power spectrum,

$A'(l)$ is an estimate of the autocorrelation function of a transparency, and

$\varphi(l)$ is the product function.

Now, the autocorrelation function in the radar experiment was computed on the basis of a maximum of 36 lags. This implies that $m = 36$. Correspondingly the total shift, L, (See Fig. 4.7) of the autocorrelation function $A(l)$ is divided into 36 equal parts and the amplitudes of the function at these points yield the desired estimate. Thus one may express:

$$A'(l) = \sum_{i=1}^{36} A_i(l) + A_0(l) = A_0 + \sum_{i=1}^{35} A_i + A_{36} \;. \qquad (5.2)$$

The product function chosen is thus:

$$\phi(l) = \frac{1}{2}\left(1 + \cos\tfrac{\pi}{36} l\right) \;, \quad |l| < 36$$

and $\qquad 0 \quad$ otherwise.

Fig. 5.1 shows a plot of $\varphi(l)$ versus . Again, L is divided into 36 equal parts and the amplitudes of $\varphi(l)$ at these points of division given in Table 5.1 are used to evaluate Eq. 5.1.

Fig. 5.1 A plot of the product functions
$\Phi(\xi)$ versus ξ
and
$\Phi(\xi) = \left(1 - \frac{\xi^2}{2}\right)^{-1/2}$
otherwise
$\Phi(\xi) = 0$
NORMALIZED AMPLITUDE
0.1
0.8
0.9
1.0
1.1
0
4
8
12
16
20
24
28
32
36

Eq. 5.1 which yields the desired power spectrum is evaluated by numerical methods wherein the integral is approximated by a summation. Thus one may write:

$$Q'(\omega) = \lim_{\Delta l \to 0} \left[(A_o \phi_o) \Delta l + 2 \sum_{i=1}^{35} A_i \phi_i \cos(\omega \Delta l \cdot i) \Delta l + [A_{36} \phi_{36} \cos(36 \omega \Delta l)] \Delta L \right] \quad (5.3)$$

where $\Delta l = \frac{L}{36}$;

or,

$$Q'(\omega) \cong \Delta l \left[A_o \phi_o + 2 \sum_{i=1}^{35} A_i \phi_i \cos(\omega \Delta l \cdot i) + A_{36} \phi_{36} \cos(36 \omega \Delta l) \right]. \quad (5.4)$$

It was indicated in Chapter II that that power spectrum is given in terms of a frequency unit called the yule, where, the yule is defined as equal to $\frac{\pi}{36}$ radians per shift. This implies that $\omega \Delta l \cdot i = \frac{\pi}{36} \cdot yi$. Correspondingly the argument of the cosine term in Eq. 5.4 changes if the same is used to obtain the power spectrum in terms of yules. Thus from Eq. 5.4 it follows that:

$$Q'(y) \cong \Delta l \left[A_o \phi_o + 2 \sum_{i=1}^{36} A_i \phi_i \cos\left(\frac{\pi}{36} yi\right) + A_{36} \phi_{36} \cos \pi y \right], \quad (5.5)$$

$$= \Delta l \left[Q_o' + 2 \sum_{i=1}^{35} Q_i'(y) + Q_{36}'(y) \right] ;$$

where $Q_o'(y) = A_o \varphi_o$, $Q_i'(y) = A_i \varphi_i \cos(\frac{\pi}{36} \cdot iy)$ and $Q_{36}'(y) = A_{36} \varphi_{36} \cos \pi y$.

The power spectrum is computed in terms of yules from Eq. 5.5. Table 5.2 shows a typical data reduction sheet used to obtain the Fourier Transform of an autocorrelation function of a transparency by using Eq. 5.5.

Three sets of transparencies (Nos. 37-30L, 32-26L, and 32-29L, Appendix, Table A.3) representing farmland, industrial and residential areas were used for correlation studies. The autocorrelation functions of the same and plots of the corresponding power spectrums obtained are included in the following pages of this chapter. The power spectra have been plotted along with the corresponding variance spectra in order that the two may be compared for each type of terrain.

DATA REDUCTION TABLES

AND RESULTS

51

TABLE 5.1

i	$\varphi(l)$	i	$\varphi(l)$
0	1	19	.4980
1	.995	20	.4130
2	.993	21	.3705
3	.988	22	.3290
4	.970	23	.2885
5	.953	24	.2500
6	.9335	25	.2130
7	.9095	26	.1785
8	.8830	27	.1465
9	.8536	28	.1170
10	.8215	29	.0900
11	.7870	30	.0665
12	.7500	31	.0475
13	.7115	32	.0300
14	.6710	33	.012
15	.6295	34	.007
16	.5870	35	.005
17	.5400	36	0
18	.5000		

TABLE 5.2 y=3 Film or run #37-30L

i	$\varphi(l)$	A_i	$\cos(\frac{\pi}{36}\cdot yi)$	$Q'_i(y) = \varphi_i A_i \cos(\frac{\pi}{36}\cdot iy)$
0	1.0000	1.0000	1.0000	1.0000
1	.9950	.8900	0.9760	.08643
2	.9930	.8400	0.8667	.72290
3	.988	.8250	0.7071	.49380
4	.9700	.8100	.5000	.39290
5	.9530	.7870	.2590	.19420
6	.9335	.7750	0	0
7	.9095	.7650	-.2590	-.18023
8	.8830	.7550	-.5000	-.33333
9	.8536	.7500	-.7071	-.4527
10	.8215	.7450	-.8667	-.53040
11	.7870	.7200	-.9760	-.5530
12	.7500	.7050	-1.000	-.5288
13	.7115	.6950	-.9750	-.48261
14	.6710	.6800	-.8667	-.39550
15	.6295	.6650	-.7071	-.2960
16	.5870	.6650	-.5000	-.19520
17	.5400	.6850	-.2590	-.08871
18	.5000	.7000	0	0
19	.4980	.7200	.2590	.09288
20	.4130	.7410	.5000	.15301
21	.3705	.7600	.7071	.19910
22	.3290	.7700	.8667	.21950
23	.2885	.7800	.9760	.21965
24	.2500	.7680	1.000	.19200
25	.2130	.7800	.9760	.16220
26	.1785	.7910	.8667	.12240
27	.1465	.7750	.7071	.08029
28	.1170	.7550	.5000	.04217
29	.0900	.7250	.2590	.01690
30	.0665	.6900	0	0
31	.0475	.6300	-.2590	-.0032
32	.0300	.5250	-.5000	-.0075
33	.0120	.435	-.7071	-.0037
34	.007	.3000	-.8667	-.0020
35	.0050	.0910	-.9760	-.0045
36	0	.0450	-1	0

$$Q'(y) = \Delta l \left[Q'_o(y) + 2 \sum_{i=1}^{35} Q'_i(y) + Q'_{36}(y) \right] = 1.2224\ \Delta l\ .$$

$$Q'(o) = \Delta l \left[Q'_o(o) + 2 \sum_{i=1}^{35} Q'_i(o) + Q'_{36}(o) \right] = 27.4995\ \Delta l\ .$$

Thus $Q'(y)$ normalized $= \frac{Q'(y)}{Q'(o)} = .044$

Fig. 5.2. Autocorrelation function of a true-parent film of run No. 32-290.
Area: Residential
Zone 1
Scale: 1 inch = 566.7 meters
NORMALIZED AMPLITUDE
1.0
0.8
0.6
0.4
0.2
0
0.2
0.4
0.6
0.8
1.0
1.2
1.4
1.6
1.8
2.0
2.2
SHIFT IN INCHES

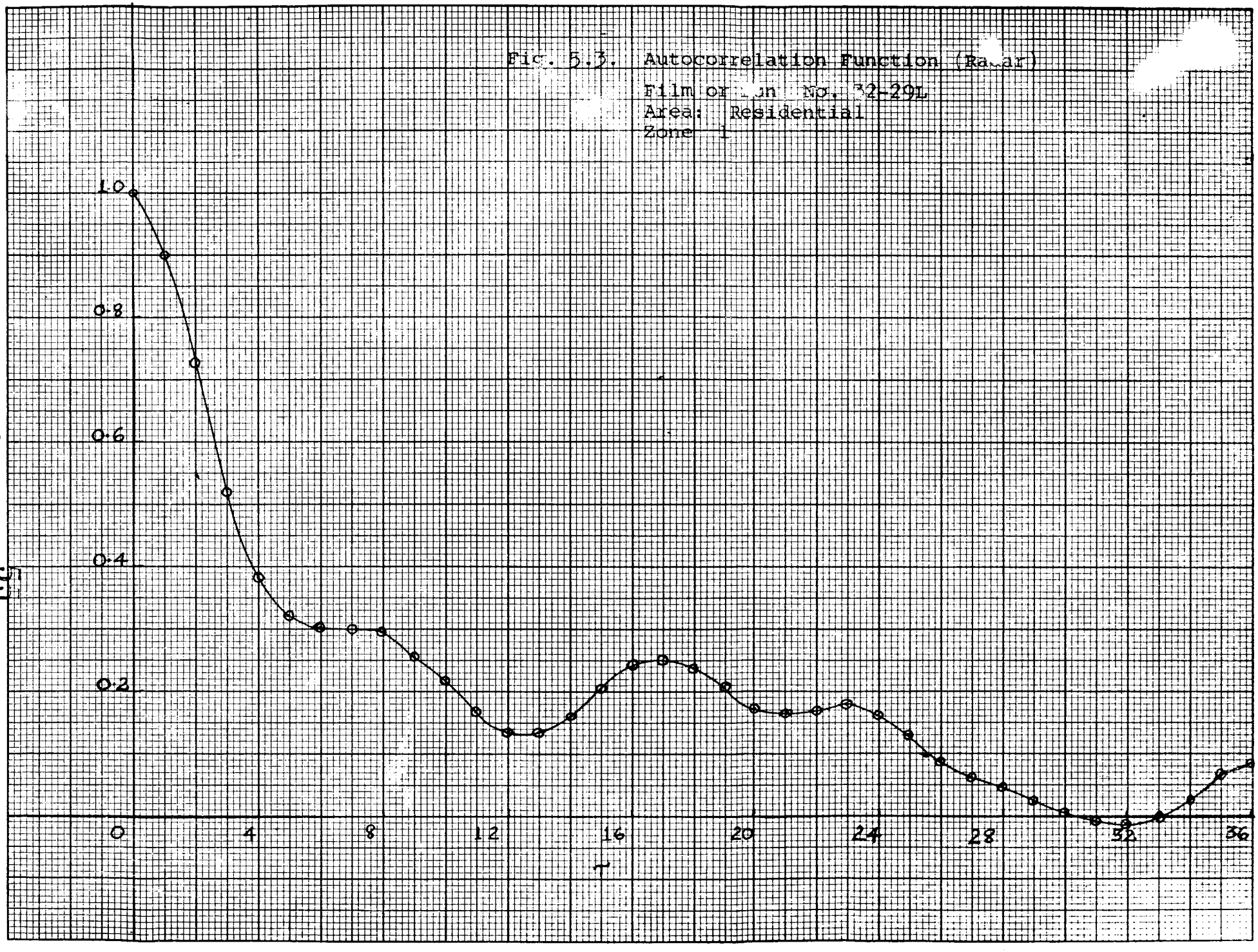
Fig. 5.3. Autocorrelation Function (Ra.ar)
Film or .on No. 32-29L
Area: Residential
Zone 1
1.0
0.8
0.6
0.4
0.2
0
4
8
12
16
20
24
28
32
36
τ

Fig. 5.11. Variance and Power Spectra
A. Variance spectrum
B. Power Spectrum
Film or Fan No. 32-295
Area: Residential
Zone 1
Scale: 1 inch = 5667 meters
NORMALIZED AMPLITUDE
0.32
0.24
0.16
0.08
A
B
0
5
10
15
YARDS

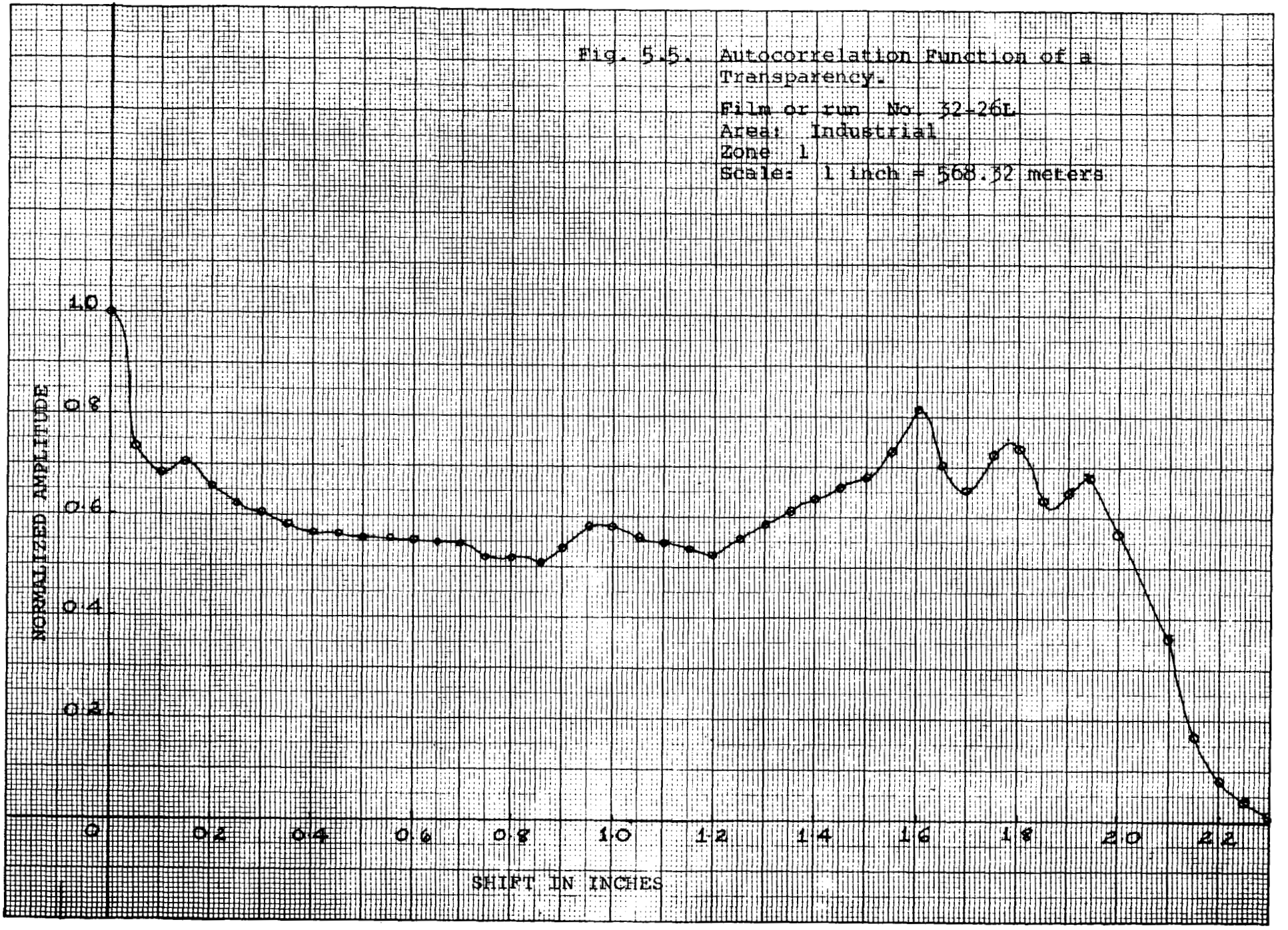

Fig. 5.5. Autocorrelation Function of a Transparency.

Film or run No. 32-26L
Area: Industrial
Zone 1
Scale: 1 inch = 568.32 meters

54

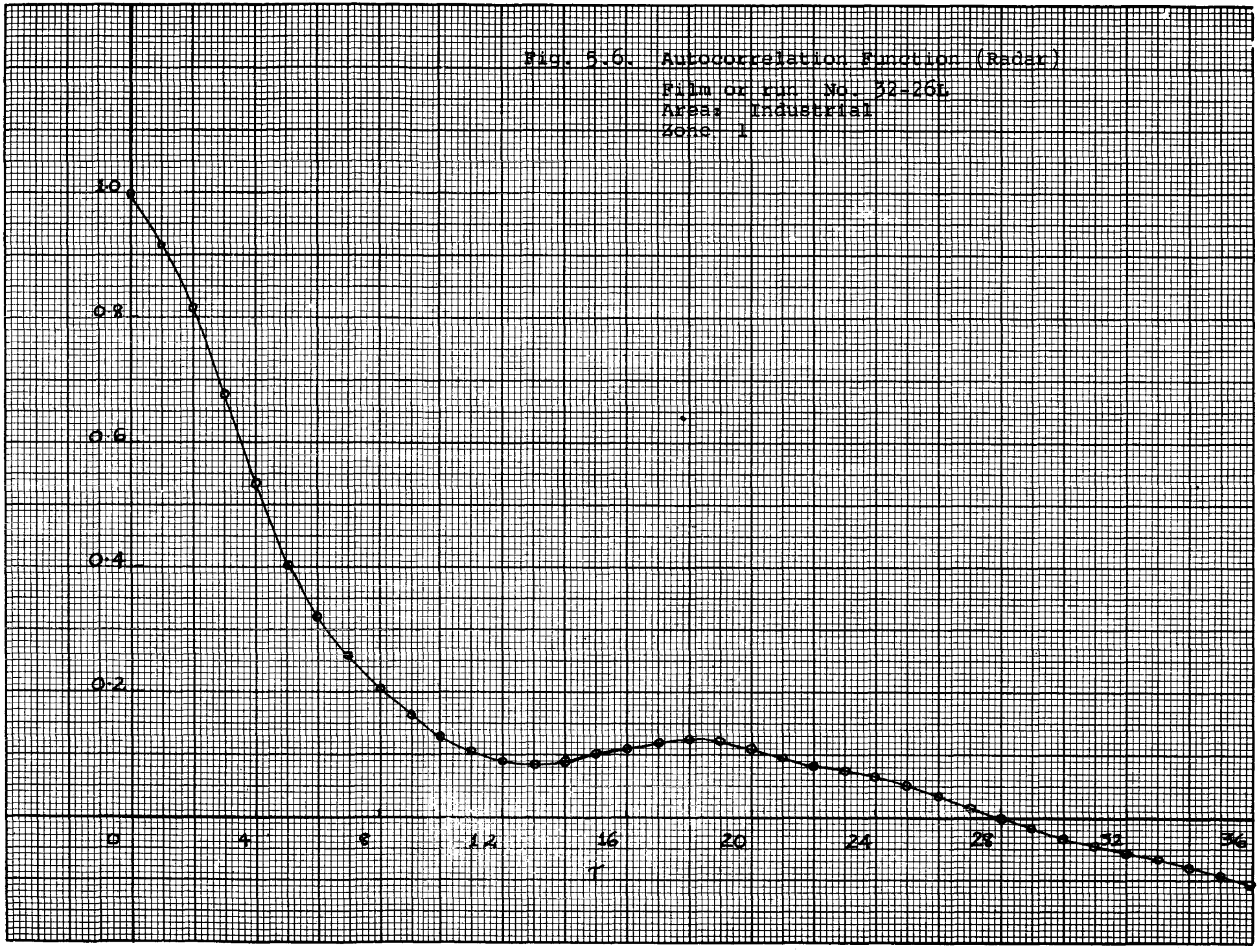
Fig. 5.6. Autocorrelation Function (Radar)
Film or run No. 32-26L
Area: Industrial
Zone 1
1·0
0·8
0·6
0·4
0·2
0
4
8
12
16
20
24
28
32
36
τ

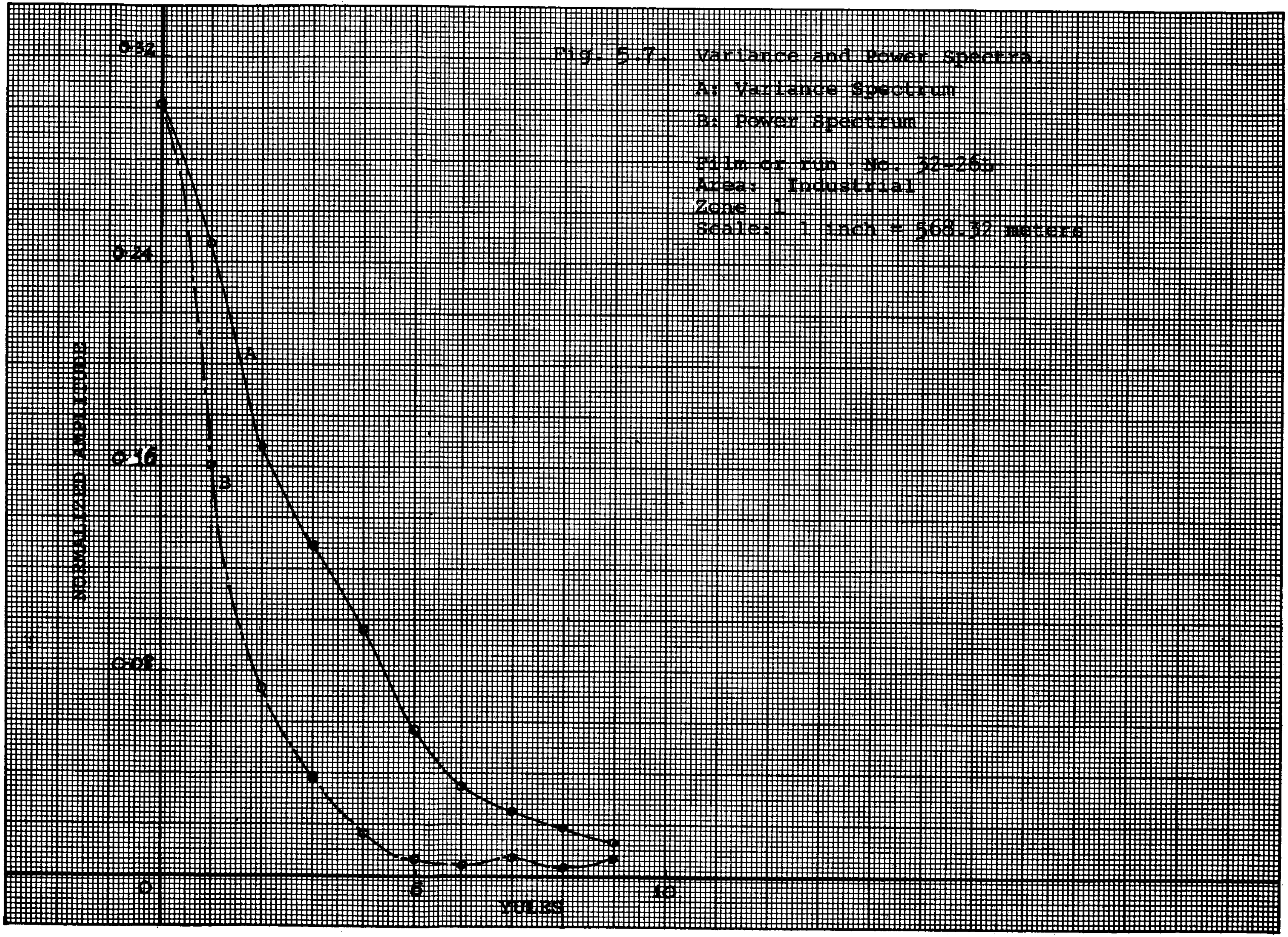

Fig. 5.7. Variance and Power Spectra.

A: Variance Spectrum

B: Power Spectrum

Film or run No. 32-265
Area: Industrial
Zone 1
Scale: 1 inch = 568.32 meters

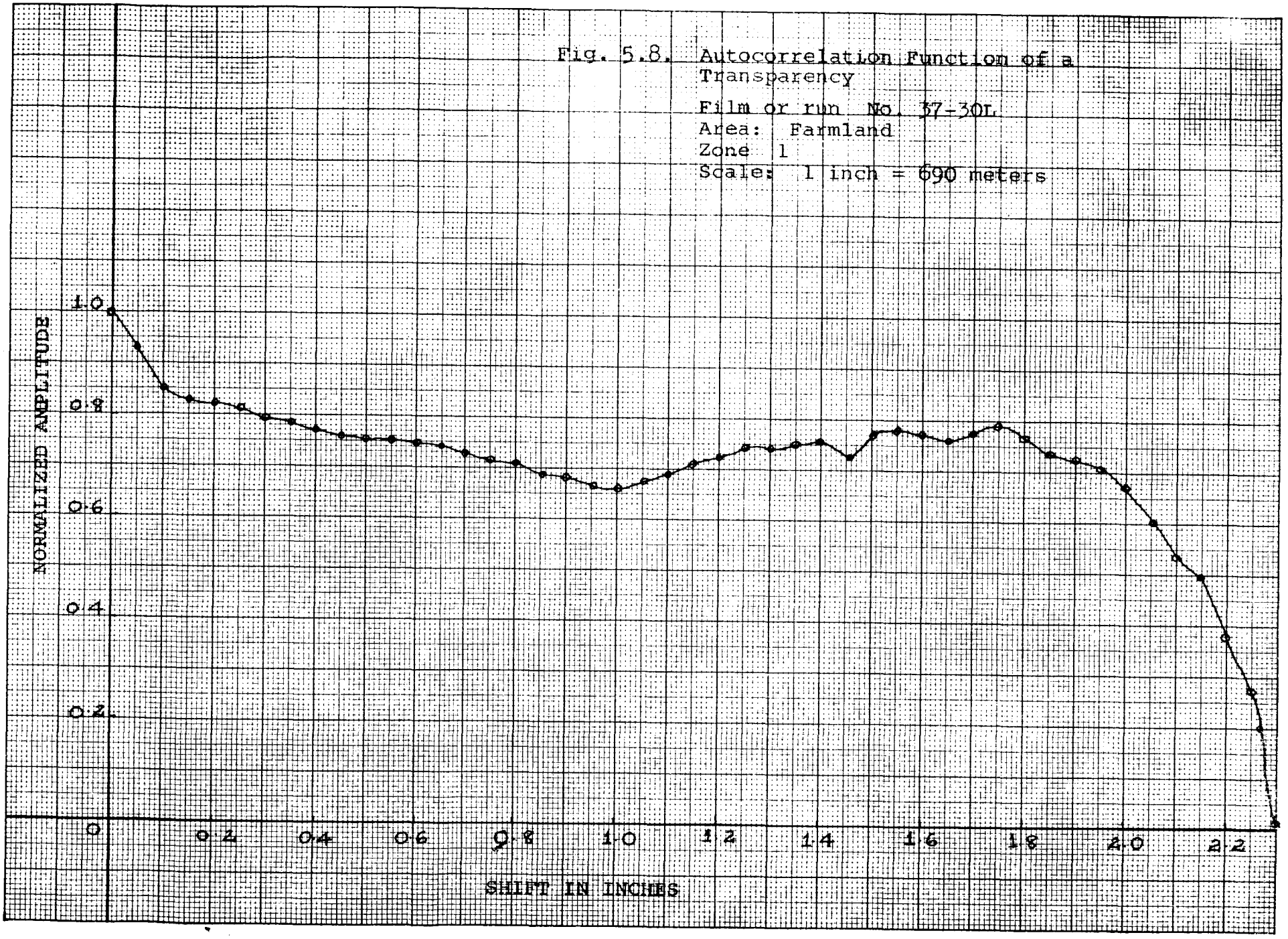

Fig. 5.8. Autocorrelation Function of a Transparency

Film or run No. 37-30L
Area: Farmland
Zone 1
Scale: 1 inch = 690 meters

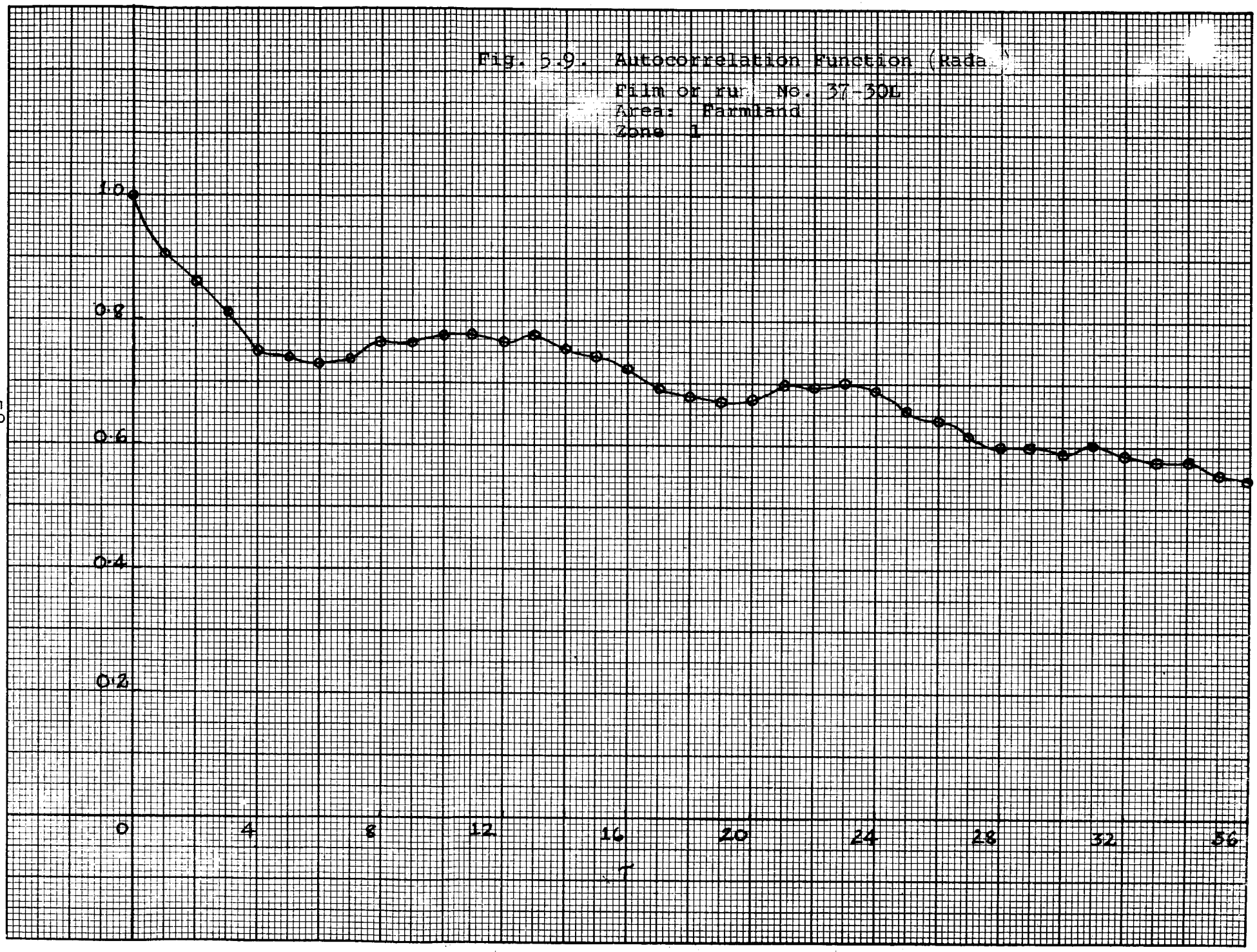
Fig. 5.9. Autocorrelation Function (Rada
Film or rur No. 37-30L
Area: Farmland
Zone 1
1.0
0.8
0.6
0.4
0.2
0
4
8
12
16
20
24
28
32
36
T

61

Fig. 5.10. Variance and Power Spectra
A: Variance Spectrum
B: Power Spectrum
Film or run no. 37-30J
Area: Farmland
Zone 1
Scale: 1 inch = 600 meters

62

CHAPTER VI
CONCLUSIONS

The results presented in the last chapter show that there is a strong correlation between the variance and power spectra for a farmland, while the correlation for the spectra obtained from residential and industrial areas is relatively weak. This may lead one to believe that a correlation between radar and photographic data on such a basis is a function of the nature of the terrain. However it is felt that in order to make any definite statement regarding the extent to which the correlation of these spectra depends on the type of terrain, further investigations of this nature are necessary.

At present only an intutive approach is available to explain the results obtained. One factor which may have obscured correlation effects in the case of the industrial and residential areas is the presence of shadows in these areas. These shadows could result from structures, trees, etc. Again, the presence of certain resonant conditions prompted by corners of buildings, etc. may have the overall effect of obscuring correlation.

However it is felt that the approach used for correlation studies in this thesis suggests further investigations in this area. These investigations may be carried out by means of the apparatus that has been presently used. A differential amplifier is the only additional unit required, and is included in the output stage of the photomultiplier tube as shown in Fig. 6.1:

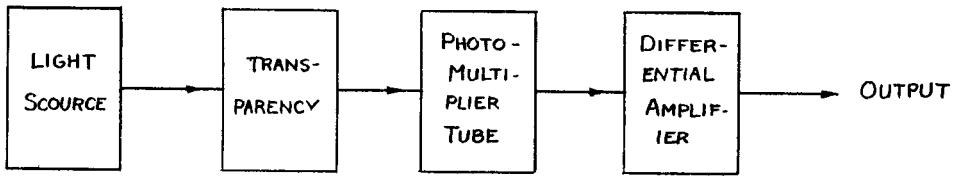

Fig. 6.1. Block Diagram Showing a Differential Amplifier with the Picture Correlator.

With the apparatus shown in Fig. 6.1, it is hoped that one may correlate the shape of a radar returned pulse, i, with the density of transmittance of that portion of the transparency that corresponds to this pulse. This can be accomplished by obtaining the responses of the photomultiplier tube corresponding to the various zones of pulse, i. Then a plot of normalized transmittance or density versus time delay corresponding to these zones may be obtained. Such a plot may have the form indicated in Fig. 6.2.

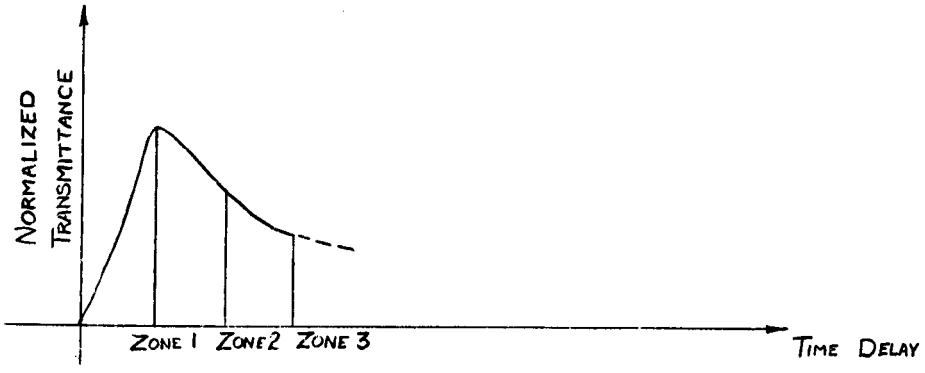

Fig. 6.2. A Plot of Normalized Transmittance Versus Time Delay Corresponding to the Illuminated Zones of Pulse, i .

The shape of the pulse constructed in this manner may then be compared to that of the radar returned pulse.

Again, the shifting mechanism may be used in another experiment which is related to obtaining a probability distribution for a photographic experiment. Here, by working with the areas corresponding to zones 1, 2, etc. of a given transparency, individual distribution curves for these zones may be obtained. In the radar experiment, the probability distribution is a measure of the variation of the power levels in the returned pulse with respect to the time variable, t . Similarly in the photographic experiment, such a distribution will represent the variations of the density or transmittance with respect to the shift variable, l . The statistics associated with the distributions of these systems may then be compared.

Thus in conclusion, it may be said that with the aid of the basic correlation studies conducted in this thesis and with those in the suggested future investigations, one may expect the development and justification of a reasonable model for the photographic experiment.

BIBLIOGRAPHY

1. Blackman, R.B. and Tukey, J.W. "The Measurement of Power Spectra" Dover Publications Inc., 1958, pp. 14-15.

2. Davies, I.L. "On Determining the Presence of Signals in Noise" Proc. Inst. Elec. Engrs., Vol. 99, Part III, 49(1952), pp. 45-61.

3. Edison, A.R., Moore, R.K., Warner, B.D., "Radar Return at Near-Vertical Incidence" Engr. Exp. Station, Univ. of New Mexico Tech. Rept. EE-24, Sept. 1959.

4. Edison, A.R. "Radar Terrain Statistics at Near-Vertical Incidence" Engr. Exp. Station, Univ. of New Mexico Tech. Rept. EE-35, Oct 1960.

5. Elias, P. "Optics and Communication Theory" Jour. of the Optical Soc. of America, Vol. 43, No. 4, April 1953, pp 229-332.

6. Felgett, P. "Concerning Photographic Grain, Signal-to-Noise Ratio, and Information" Jour. of the Optical Soc. of America, Vol. 43, No. 4, April 1953, pp 271-282.

7. Gragg, D.M. "Target of Terrain Return Project" Sandia Corp. Tech. Memo, No. 57-55-54, April 1955.

8. Gragg, D.M. "Target of Terrain Return Project" Sandia Corp. Tech. Memo, No. 58-55-54, April 1955.

9. Kretzmer, E.R. "Statistics of Television Signals" Bell System Technical Jour., Vol. 31, July 1952, pp 751-763.

10. Lee, L.W. "Statistical Theory of Communication" Wiley Publication, Chapter I, 1960.

11. Linfoot, E.H. and Felgett, P.B. "On Assessment of Optical Images" Trans. Royal Soc. (London), 247, Feb 1955.

12. O'Neil, E.L. "Selected Topics in Optics and Communication Theory" Physical Res. Lab., Boston Univ. Tech. Note No. 133, pp 25-28.

13. Welch, P.D. "Interpretation and Prediction of Radar Terrain Return Fading Spectra" New Mexico ANM, Physical Science Lab. Rept. AER-14-W, May 1955.

14. Williams, C.S., Jr., Bidwell, C.H., Gragg, D.M., "Radar Return from the Vertical for Ground and Water Surfaces" SER-107, April 1960.

APPENDIX

DATA AVAILABLE FOR CORRELATION STUDIES

The data in which correlation studies have been conducted was part of an experimental program to investigate the reradiation properties of terrain at near-vertical incidence. This program was initially carried out by the Sandia Corporation[1].

The approximate characteristics of the two radars used in obtaining the data are given in Table A.1.

TABLE A.1

	No. 1	No. 2
Frequency	415 Mcps.	3800 Mcps.
Pulse Width	0.1 micro-sec.	0.2 micro-sec.
Antenna Gain	5 db	12 db

More detail concerning the pulse shapes and antenna patterns is given in Part III in Figs. 111-1 through 111-5 of the concerned report.

While obtaining the data, the radars were carried by a 130-knot aircraft that made straight and level runs, each of several seconds duration, over some 31 individual terrains that may be categorized into 17 general types. The antennas were directed straight down. Over most of the terrains, data

[1] Williams, C.S., Jr., Bidwell, C.H., and Gragg, D.M. "Radar Return from the Vertical for Ground and Water Surfaces" SER-107, April 1960.

were taken at four altitudes: approximately 600, 1200, and 3000 meters (2000, 4000, 7000, and 12,000 feet) above the ground. The effects of polarization of the transmitted wave were ignored.

The thirty-one specific terrains over which data were taken may be categorized as shown in Table A.2.

TABLE A.2

Serial Number	Type	Description
1	A	Water, smooth
2	B	Water, ocean
3	C	Water, frozen lakes
4	D	Water, rippled
5	E	Farmland
6	F	Orchard
7	G	Farmland with snow
8	H	Forest
9	J	Forest with snow
10	K	City, residential with snow
11	L	City, residential
12	M	City, industrial with snow
13	N	City, industrial
14	P	Dry desert, some vegetation
15	R	Dry desert, bare
16	S	Sand hills
17	T	Sand flats

For the purposes of correlation studies, terrains from the categories E, L, and N are considered. Brief descriptions pertaining to these terrains will now be given. For more

details one might refer to Sandia Corporation Technical Memoranda[1] (SCTM) whose numbers are listed in Table A.3.

Type E. Farmland: Imperial Valley of California.

This terrain consists of a cultivated and irrigated farmland covered with heavy growth of pasture and grasslike crops. The irrigation is sufficient to cause the ground to be rather wet. Fig. 3.3 (Chapter III) is an aerial photograph of the terrain.

Type L. Residential: Minneapolis, Minnesota.

The terrain has been shown in Fig. A.1. It consists of one and two story brick and frame structures with pitched roofs. Flat roofed apartment houses, schools, and business houses are scattered throughout the area. Streets, with a few exceptions, are paved with the main thoroughfares having rails for streetcars embedded in them. The trees are old, well established, as high or higher than the houses. The area in general is flat. Some steep rises of perhaps 50 feet in the course of a block occur. A maximum variation of 100 feet may be safely assumed for the elevations within the target area.

Type N. Industrial: St. Paul, Minnesota.

An aerial photograph of the terrain is given in Fig. 3.5 (Chapter III). The factory buildings are all very large and predominantly metal roofed. Some are constructed wholly of corrugated metal. Trees are scattered through the area but are by no means predominant. Very little open ground exists in the area except for a few parking lots.

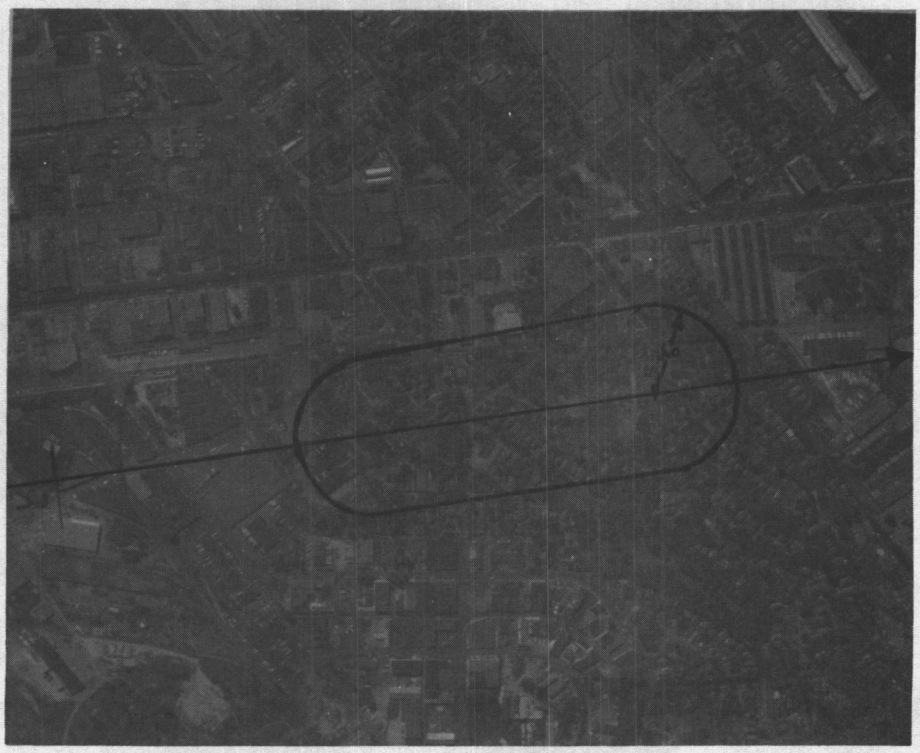

Fig. A.1. An Aerial Photograph of an Industrial Area with the Line of Flight and the Area Corresponding to Zone 1 Located on it.

TABLE A.1

Serial	Type of Terrain	Radar Freq. f_o (Mcps)	Altitude above Terrain h(feet)	Aircraft ground speed (feet per sec.)	Film or run number	Sandia Corp. Technical Memorandum Number	PSL Number
1.	E	415	3877	209.97	37-30L*	-	37-30L*
2.	L	415	3919	196.85	32-29L	58-55-54	32-29L
3.	N	415	3700	167.32	32-29L	57-55-54	32-26L

*Footnote: The letter L, indicates that the radar frequency was "low" - i.e. 415 Mcps.